Chemical Fate of Contaminants in the Environment: Chlorinated Hydrocarbons in the Groundwater

William R. Wiley
EMSL
Environmental Molecular Sciences Laboratory

B.C. Garrett
E.E. Arcia
Y.A. Borisov
C.J. Cramer
T.H. Dunning, Jr.
M. Dupuis

J. Gao
K. Morokuma
T.P. Straatsma
J. Thompson
D.G. Truhlar

August 2002

Theory, Modeling and Simulation

MSCF

Molecular Science Computing Facility

DISCLAIMER

Chemical Fate of Contaminants in the Environment: Chlorinated Hydrocarbons in the Groundwater

B.C. Garrett   J. Gao
E.E. Arcia   K. Morokuma
Y.A. Borisov   T.P. Straatsma
C.J. Cramer   J. Thompson
T.H. Dunning, Jr.   D.G. Truhlar
M. Dupuis

August 2002

Chemical Fate of Contaminants in the Environment: Chlorinated Hydrocarbons in the Groundwater

Abstract

Chlorinated hydrocarbons (CHCs) are the most common contaminant found at hazardous waste sites and are the most prevalent contaminants on (Department of Energy) DOE weapons production sites. Many of the chlorinated hydrocarbons are either known or suspected carcinogens and thus pose health risks to the public and/or site workers. Chlorinated hydrocarbons, unlike simple hydrocarbons, are resistant to biodegradation, but can degrade by abiotic processes such as hydrolysis, nucleophilic substitution, and dehydrochlorination. Unfortunately, few studies of the reactions of chlorinated hydrocarbons have been reported in the literature, and disagreement still exist about the mechanisms and rates of many of the key reactions.

In this work we modeled the reactions involved in the degradation of chlorinated hydrocarbons in the groundwater. We examined elementary reactions involved in the aqueous phase chemistry of chlorinated methanes and ethylenes in an attempt to obtain a detailed understanding of the abiotic processes involved in the degradation of this important class of contaminants. We began by studying the reactions of $CH_nCl_{(4-n)}$ and $C_2H_nCl_{(4-n)}$ with OH^-, as these are thought to be the dominant processes involved in the degradation of these chlorinated species. We used state-of-the-art theoretical techniques to model the elementary reactions of chlorinated hydrocarbons important in the groundwater. We employed high accuracy electronic structure methods (perturbation theory and coupled cluster methods with correlation consistent basis sets) to determine the energies of the various stable species, intermediates, and transition states involved in the elementary reactions of CHCs. Effects of solvation on the reaction energetics were studied by including small numbers of solvent molecules (microsolvation). The ONIOM (our own N-layered molecular orbital + molecular mechanics) method allows the number of solvent molecules to be increased and hybrid quantum mechanical/molecular mechanics (QM/MM) methods and continuum solvation models were used to estimate the effects of bulk solvation. Rate constants for the gas-phase, microsolvated, and bulk-phase reactions were computed using variational transition state theory (VTST)

Research team Members

Bruce C. Garrett, Thom H. Dunning, Jr., Michel Dupuis, Edgar E. Arcia, and Tjerk P. Straatsma
Environmental Molecular Sciences Laboratory, Pacific Northwest National Laboratory, Richland, Washington 99352

Donald G. Truhlar, Jason Thompson, Christopher J. Cramer, and Jiali Gao
Department of Chemistry and Minnesota Supercomputer Institute, University of Minnesota, Minneapolis, Minnesota 55455

Keiji Morokuma
Department of Chemistry, Emory University, Atlanta, Georgia 30322

Yurii A. Borisov
Nesmeynov Institute of Organo-Element Compounds, Russian Academy of Sciences, 117813 GSP-1, Moscow V-334, Vavilova St., 28

Financial Support

Number of Hours Allocated for the Past Three Years (Exclude Refund Deposits)

Period: 23-May-98 through 31-May-99
Allocation: 375,000 node hours

Period: 1-Jun-99 through 31-May-00
Allocation: 375,000 node hours

Period: 1-Jun-00 through 31-May-01
Allocation: 375,000 node hours

Number of Hours Actually Used in the Past Three Years (Exclude Refunded Amounts)

Period: 23-May-98 through 31-May-99
Used: 137,208 node hours

Period: 1-Jun-99 through 31-May-00
Used: 179,276 node hours
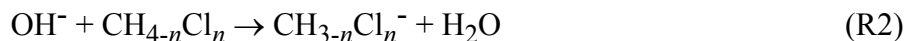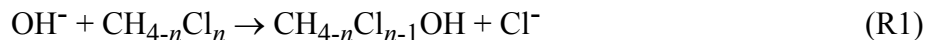
Period: 1-Jun-00 through 31-May-01
Used: 277,057 node hours

Overview Of Past Three Year's Accomplishments and Activities

The major objective of this research project was to obtain *accurate* estimates of the lifetimes of chlorinated hydrocarbons (CHCs) in an aqueous environment determined from abiotic reactions and to identify any long-lived, potentially hazardous intermediates formed from the original CHCs. Estimating CHC lifetimes requires an understanding of the reaction mechanisms for all of the major pathways and their associated rate constants. Meeting the objective of accurately estimating CHC lifetimes requires careful benchmark studies of the computational methods employed as well as applications to systems of interest. It also requires an accurate and affordable electronic structure method that considers the effects of solvation (if the solvent is modeled implicitly as a continuous medium having a bulk dielectric constant).

In this research project *ab initio* electronic structure theory was the basis for the calculation of the reaction energetics. Aqueous solvation can have profound effects on the reaction energetics and we explored the effects of solvation using a number of different techniques. First, the effects of microsolvation on the electronic structure of the reacting species were studied using accurate *ab initio* calculations for the reactions with small numbers of solvent molecules added. The approach to bulk solvation was examined by extending the microsolvation studies using the IMOMO (Integrated Molecular Orbital Molecular Orbital) method or the more general ONIOM (our own N-layered molecular orbital + molecular mechanics) method. Finally, continuum solvation models and hybrid quantum mechanical/molecular mechanics (QM/MM) methods were used to estimate the effects of bulk solvation on the reaction energetics. Rate constants for the reaction were computed using variational transition state theory (VTST).

Work on this project focused on benchmark calculations of the gas-phase reactions, microsolvation studies, ONIOM calculations, and QM/MM studies for the reactions

$$OH^- + CH_{4-n}Cl_n \rightarrow CH_{4-n}Cl_{n-1}OH + Cl^- \qquad (R1)$$

$$OH^- + CH_{4-n}Cl_n \rightarrow CH_{3-n}Cl_n^- + H_2O \qquad (R2)$$

for $n = 1$-4. Reactants, reactant complexes, transition states, product complexes, and products were characterized for the nucleophilic substitution (S_N2) reaction, (R1), and for the proton transfer reaction, (R2). Critical geometries were optimized at the MP2/aug-cc-pVDZ level of theory. Single point calculations were performed at these geometries using MP2, MP3, CCSD,

and CCSD(T) with complete basis set (CBS) estimates obtained using the aug-cc-pVxZ basis sets with x = 2,3,4. We also initiated studies of the reactions $OH^- + CH_2CH_{(2-n)}Cl_n$ at the MP2/aug-cc-pVDZ level of theory. For these gas-phase reactions OH^- abstracts a proton from the carbon atom with no chlorine atoms with no barrier to the reaction. These systems have small barriers to the elimination of Cl^- to form acetylene and a hydrated chloride ion.

During the third year of this project significant progress was made in completing the benchmark calculations for microsolvated versions of S_N2 and proton transfer reactions of OH^- with $CH_{4-n}Cl_n$

$$OH^-(H_2O)_m + CH_{4-n}Cl_n \rightarrow CH_{4-n}Cl_{n-1}OH(H_2O)_{m-m'} + Cl^-(H_2O)_{m'} \qquad (R3)$$

$$OH^-(H_2O)_m + CH_{4-n}Cl_n \rightarrow H_2O(H_2O)_{m-m'} + CH_{3-n}Cl_n^-(H_2O)_{m'} \qquad (R4)$$

Our efforts focused on the reactions of CH_3Cl and CH_2Cl_2 (e.g., $n = 1$-2) and $m = 0$-2. Using the same protocol established for the reaction with no solvation by water molecules, critical geometries were optimized at the MP2/aug-cc-pVDZ level of theory and single point calculations were performed at these geometries using MP2, MP3, CCSD, and CCSD(T) with complete basis set (CBS) estimates obtained using the aug-cc-pVxZ basis sets with x = 2,3,4. In addition, we used a two-point extrapolation formula to estimate the complete basis set limit.[1]

Minimum energy path (MEPs) have been computed at the MP2/aug-cc-pVDZ level of theory for both reactions (R1) and (R2) with $n = 1$-3 and for reaction (R1) with $n = 4$. Information along the MEPs was used in variational transition state theory (VTST) calculations of rate constants for the gas-phase reactions and compared with experimental values for reaction (R1) with $n = 1$. Since the saddle point energy is below the reactant asymptote for the reaction, we have calculated the MEP in the entrance channel for the reaction, to allow VTST calculations of the bimolecular rate constants. These calculations indicate that gas-phase rate constants for reaction (R1) with $n = 1$-3 are controlled by dynamical bottlenecks in the entrance channel, while reaction (R1) with $n = 4$ has the dynamical bottleneck near the saddle point. The computed rate constants are in good agreement with experimental values.

Calculations of MEPs were also extended to the microsolvated reactions (R3) and (R4). The MEPs were computed for the entrance channels as well as near the saddle points to compare the locations of the dynamical bottlenecks with those for the gas-phase reactions. For reaction (R1) the energy of the saddle point (relative to the asymptotic reactant energy) increases upon microsolvation and the dynamical bottleneck switches from the entrance channel to the saddle point. The calculated rate constants for the microsolvated reactions therefore are a better benchmark (than the gas-phase reaction rates) of the region of the potential that controls the rate of the bulk phase reaction.

The two-layered ONIOM method was examined for the investigation of the S_N2 reaction pathway (reactants, reactant complexes, transition states, product complexes and products) between CH_3Cl and OH^- ion in micro-solvation clusters with one or two water molecules. Only

---

[1] Y. A. Borisov, E. E. Arcia, S. L. Mielke, B. C. Garrett, and T. H. Dunning, Jr., J. Phys. Chem. A (in press).

the solute part, CH_3Cl and OH^-, was treated at a high level of molecular orbital (MO) theory and all solvent water molecules at a low MO level. The ONIOM calculation at the MP2(Møller-Plesset second order perturbation)/aug-cc-pVDZ (augmented correlation-consistent polarized valence double zeta basis set) level of theory as the high level coupled with the B3LYP (Becke3 parameter-Lee-Yang-Parr) /6-31+G(d) as the low level was found to reasonably reproduce the "target" geometries at the MP2/aug-cc-pVDZ level of theory. The present results indicate that the ONIOM method would be a powerful tool for obtaining reliable geometries and energetics for chemical reactions in larger micro-solvated clusters with a fraction of cost of the full high level calculation, when an appropriate combination of high and low level methods is used. The importance of careful test is emphasized.

A multitude of electronic structure methods could be used to model the reactions of CHCs, but many of these methods are too computationally demanding for use in calculations including solvent (either explicitly with QM/MM methods or implicitly using continuum models). A significant portion of our efforts over the past year were focused on finding accurate and affordable electronic structure methods such as hybrid Hartree-Fock-density-functional (HF-DF) methods to model the various processes of CHCs in an aqueous medium. First, we have studied the two gas-phase reactions (R1) with $n = 1$ and 2.

For reaction (R1) with $n = 1$, we have optimized critical geometries such as the reactants, products, reactant complex, and saddle point at two hybrid HF-DF levels of theory using several basis sets, namely MPW1K/6-31+G(d), MPW1K/6-31+G(d,p), MPW1K/MG3, MPW1KK/6--31+G(d), MPW1KK/6-31+G(d,p), and MPW1KK/MG3. The MPW1K level of theory is a hybrid HF-DF method that uses a modified version of Perdew and Wang's exchange density functional, Perdew and Wang's correlation-energy density functional, and a fraction of HF exchange of 0.428.[2] The MPW1KK level of theory uses the same exchange and correlation density functionals as MPW1K and a fraction of HF exchange of 0.606. The performance of these methods has been evaluated by comparing the energetics of reaction (R1) with n=1 to very accurate, but more expensive methods such as MP2/MG3, MC-QCISD, and MC-G3. We note that the MG3 basis is an improved basis set of 6-311++G(3d2f,2df,2p)-type that we have found to perform better for second-row atoms than correlation-consistent basis sets like aug-cc-pVTZ because it has tighter d functions.

For reaction (R1) with $n = 2$, we have optimized geometries of the reactants, products, and saddle point at the MPW1K and MPW1KK levels of theory using the 6-31+G(d) and 6-31+G(d,p) basis sets. We have evaluated the performance of these methods by comparing the energetics of this reaction to the MP2/MG3 level of theory.

To see how robust these hybrid HF-DF methods are for other similar types of reactions, we have also studied the stepwise enthalpy of hydration of the chloride and hydroxide ions, *i.e.*,

$$OH^- + H_2O \rightarrow [OH(H_2O)]^- \tag{R5}$$

$$Cl^- + H_2O \rightarrow [Cl(H_2O)]^- \tag{R6}$$

---

2   B. J. Lynch, P. L. Fast, M. Harris, and D. G. Truhlar, Journal of Physical Chemistry A **104**, 4811-4815 (2000).

at the MPW1K and MPW1KK levels of theory using the 6-31+G(d) and 6-31+G(d,p) basis sets. We have compared these results to those obtained at the MP2/MG3 level of theory and to experimental results, where available.

Finally, we have investigated electron affinities of the chlorine atom and the hydroxyl radical. These electron affinities have been calculated at the MPW1K and MPW1KK levels of theory using the 6-31+G(d), 6-31+G(d,p), and MG3 basis sets. We have compared these results to the MP2/MG3 level of theory and to experimental results.

A combined ab initio QM/MM approach was used to study the decomposition of CCl_3^- in water. This reaction is a key step in the decomposition of chloroform in aqueous solution. The solvent was found to play a major role in accelerating the decomposition reaction in water in comparison with the gas phase process.

A combined ab initio QM/MM approach was also applied to compute the potential of mean force for the S_N2 reaction $OH^- + CH_3Cl$. The reactants OH^- and CH_3Cl were treated quantum mechanically at the Hartree-Fock (HF) level of theory, and basis sets from STO-3G through 6-31G* were tested. The solvent molecules were treated using the TIP3P water potential with the water-reactant interactions given by site-site Lennard-Jones interactions and interactions of the charge distribution of the reactants with the charges on the solvent molecules. The self-consistent field (SCF) solution of the electronic structure for the reactants in the field of the charges on the solvent molecules must be repeated for each new solvent configuration. Computational methods were explored to efficiently sample the QM potential based upon configurations generated with a MM model of the reactants as well as the solvent. The point charges of the reactants were fitted to reproduce the electrostatic potential of the reactants and they change as the reactant geometries change along the MEP. The implementation of QM/MM in the HONDO program (Dupuis) was adapted to run in parallel on the MPP for these calculations.

Publications

Y. Mo, J. Gao, "Ab Initio QM/MM Simulations with a Molecular Orbital-Valence Bond (MOVB) Method : Application to an SN2 Reaction in Water." J. Comp. Chem. **21**, 1458-1469 (2000).

S. Re and K. Morokuma; "ONIOM Study of Chemical Reactions in Microsolvation Clusters: $(H_2O)_nCH_3Cl + OH^-(H_2O)_m$ (n + m = 1 and 2), J. Phys. Chem. A **105**, 7185-7197 (2001).

Y. A. Borisov, E. E. Arcia, S. L. Mielke, B. C. Garrett, and T. H. Dunning, Jr., "A Systematic Study of the Reactions of OH^- with Chlorinated Methanes: 1. Benchmark Studies of the Gas-Phase Reactions" J. Phys. Chem. A (in press)

Presentations

<u>Invited Presentations</u>

B. C. Garrett, "Molecular Approaches to Chemical Kinetics: from Gas to Condensed Phases," Chemistry Department, University of Montana, Missoula, Montana, November 22, 1999.

"Ab initio combined QM/MM simulation of chemical processes in solution", **13th Canadian Symposium on Theoretical Chemistry**, The University of British Columbia, Vancouver, British Columbia, August 2-7, 1998.

<u>Contributed Presentations (Oral and Poster)</u>

E. E. Arcia, "Direct Dynamics Study of the Reaction Path and Rate Constants of $OH^- + CH_3Cl \rightarrow Cl^- + CH_3OH$," Northwest Regional Meeting of the American Chemical Society, Portland, Oregon, June 21-23, 1999.

E. E. Arcia, "Direct Dynamics Study of the Reaction Path and Rate Constants of $OH^- + CH_3Cl \rightarrow Cl^- + CH_3OH$," American Conference on Theoretical Chemistry, Boulder, CO, June 28 – July 2, 1999.

E. E. Arcia, "A Systematic Study of the Reactions of OH- with Chlorinated Methanes," Joint 55th Northwest/16th Rocky Mountain Regional Meeting of the American Chemical Society, Idaho Falls, Idaho, June 15-17, 2000.

J. D. Thompson, C. J. Cramer, and D. G. Truhlar, "Reactions of Hydroxide with Chlorinated Hydrocarbons", 34th Midwestern Theoretical Chemistry Conference, Minneapolis, Minnesota, October 5-6, 2001.

E. E. Arcia, "Theoretical rates of gas-phase reactions of OH- with chlorinated methanes," Northwest Regional Meeting of the American Chemical Society, Seattle, WA, June 14-17, 2001.

E. E. Arcia, "Theoretical rates of gas-phase reactions of OH- with chlorinated methanes," 2001 West Coast Theoretical Chemistry Conference, Davis, CA, June 21-23, 2001.

Methods/Routines or Codes Developed

<u>Parallel Implementation Of PMF Calculations Using QM/MM</u>

The Metropolis Monte Carlo (MC) algorithm was implemented in HONDO to perform equilibrium ensemble averages for constrained geometries of the reactants. The code was adapted to run on any number of nodes on the MPP. The implementation generates independent initial random configurations of the solvent water molecules on each node. Independent calculations MC simulations are performed on each node, with the resulting data sets being combined and averaged at the end of the job.

Appendix A — Full Report of First Year Activities and Accomplishments

Benchmark Ab Initio Electronic Structure Calculations

Extensive benchmark calculations have been performed on the reaction energies for reactions (R1) and (R2). Tables 1 and 2 summarize the results for the reactions with $CH_{4-n}Cl_n$, with n=1-4. The most detailed calculations were performed for CH_3Cl and these results are depicted in Figures 1 and 2.

Values of the extrapolations to the complete basis set (CBS) limit listed in Tables 1 and 2 and plotted in Figures 1 and 2 are obtained as follows. The total energy for each reactant (e.g., OH^-, CH_3Cl, etc.) and product (e.g., Cl^-, CH_3OH, etc.), which are monotonically decreasing functions of the basis set size (x) are extrapolated using the functional form $E_\infty + A (x+1/2)^4 + B (x+1/2)^5$, where x = 2, 3, 4 for the aVDZ, aVTZ, and aVQZ basis sets, respectively. The CBS value for the reaction energies are obtained from the CBS values for each reactant and product. The MPn series is not well converged with respect to increasing n and for the S_N2 reaction appears that it may be divergent. For the S_N2 reaction the only extrapolation lying within the experimental range is that for CCSD(T). For the proton transfer reaction, all the results lie within the large experimental uncertainty, but the CCSD(T) results are the closest to the best experimental estimate. It is also interesting that the dependence on basis set for all the methods are all very similar. Therefore, it will be instructive to examine differences between these methods, since differences may converge more rapidly with respect to basis set than the individual components.

Table 1. Reaction energetics (in kcal/mol) for the S_N2 reaction (R2) of OH^- + $CH_{4-n}Cl_n$. The basis sets aVxZ denote the aug-cc-pVxZ basis sets, CBS denotes extrapolation to the complete basis set limit, and ZPE denotes a harmonic approximation to the zero point energy.

	CH_3Cl	CH_2Cl_2	$CHCl_3$	CCl_4
MP2/aVDZ	-51.68	-59.19	-64.51	-65.86
MP2/aVTZ	-49.15	-56.58	-61.73	-63.37
MP2/aVQZ	-49.30	-56.71	-61.85	-63.38
MP2/CBS	-49.74	-57.12	-62.27	-63.65
MP3/aVDZ	-58.18	-66.27	-72.42	-74.83
MP3/aVTZ	-56.58	-64.75	-70.85	-73.62
MP3/aVQZ	-57.27	-65.47	-71.59	-74.26
MP3/CBS	-58.19	-66.41	-72.55	-75.06
MP4/aVDZ	-49.82			
MP4/aVTZ	-47.75			
CCSD/aVDZ	-55.45	-63.20	-68.82	-70.70
CCSD/aVTZ	-53.90	-61.71	-67.28	-69.54
CCSD/aVQZ	-54.66	-62.50	-68.10	
CCSD/CBS	-55.64	-63.50	-69.14	
CCSD(T)/aVDZ	-53.65	-61.36	-66.91	-68.60
CCSD(T)/aVTZ	-51.80	-59.58	-65.06	-67.11
CCSD(T)/aVQZ	-52.48	-60.27	-65.77	
CCSD(T)/CBS	-53.41	-61.21	-66.74	
exp ΔH_0	-50.2±1.1	-59.3±2.8	-66.4±2.6	-67.3±2.6
ZPE	3.15			

Table 2. Reaction energetics (in kcal/mol) for the proton transfer reactions (R2) of OH⁻ + $CH_{4-n}Cl_n$. The basis sets aVxZ denote the aug-cc-pVxZ basis sets, CBS denotes extrapolation to the complete basis set limit, and ZPE denotes a harmonic approximation to the zero point energy.

	CH_3Cl	CH_2Cl_2	$CHCl_3$
MP2/aVDZ	11.00	-9.41	-27.76
MP2/aVTZ	11.55	-7.96	-25.50
MP2/aVQZ	11.36	-8.26	-25.81
MP2/CBS	11.09	-8.74	-26.39
MP3/aVDZ	4.98	-15.90	-33.78
MP3/aVTZ	5.19	-14.78	-31.66
MP3/aVQZ	4.83	-15.38	-32.35
MP3/CBS	4.42	-16.14	-33.33
MP4/aVDZ	10.79		
MP4/aVTZ	11.30		
CCSD/aVDZ	7.05	-13.81	-31.50
CCSD/aVTZ	7.60	-12.29	-29.03
CCSD/aVQZ	7.30	-12.79	-29.62
CCSD/CBS	6.91	-13.48	-30.52
CCSD(T)/aVDZ	7.36	-13.72	-32.20
CCSD(T)/aVTZ	8.04	-12.23	-29.94
CCSD(T)/aVQZ	7.77	-12.74	-30.61
CCSD(T)/CBS	7.41	-13.45	-31.58
exp DH	6.9±4.9	-14.8±5.2	-32.6±7.9
ZPE	-1.49		
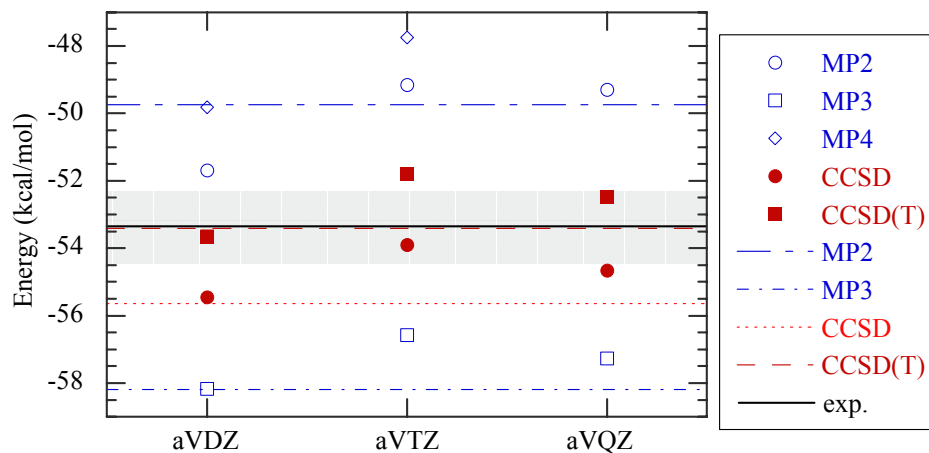
Figure 1. Basis set dependence of the reaction energy for the SN2 reaction OH- + CH3Cl CH3OH + Cl-. The aug-cc-pVxZ basis sets with x = D, T, and Q are denoted aVxZ. The dashed lines are extrapolations to the complete basis set limits. The solid line is the best estimate for the reaction energy (with the zero point energy removed) and the gray region represents the uncertainty in the experimental value.
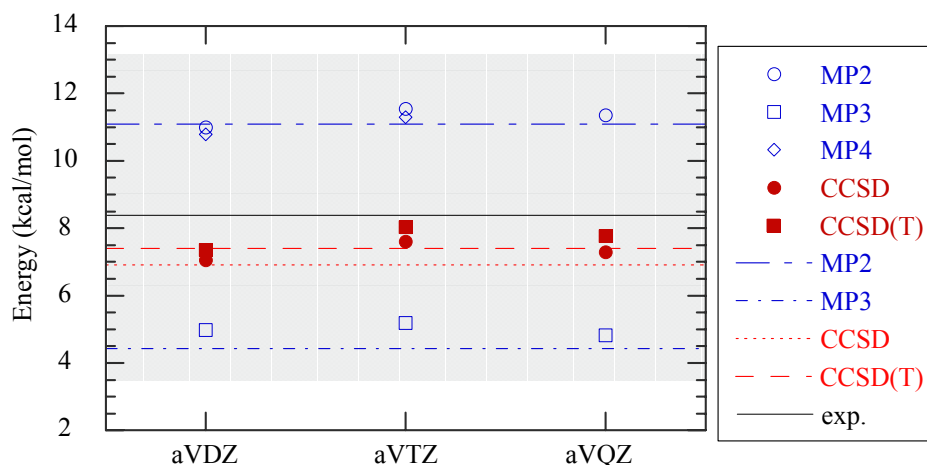
Figure 2. Same as Figure 1 except for the reaction energy of the proton transfer reaction OH- + CH3Cl   CH2Cl- + H2O.

In solution the relevant reaction barriers and rate constants are for the unimolecular reactions that proceed from reactant to product complexes. Therefore, we focus on the reactions

$$CH_{4-n}Cl_n \cdots OH^- \rightarrow CH_{4-n}Cl_{n-1}OH \cdots Cl^-$$

$$CH_{4-n}Cl_n \cdots OH^- \rightarrow CH_{3-n}Cl_n \cdots H_2O$$
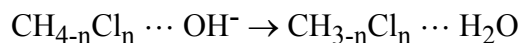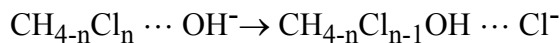
where ⋯ between species denotes a bound complex. Figure 3 shows examples of geometries of the reactant and product complexes and the transition state for these two reactions in the case that n=1. Critical geometries for the complexes and transition states have been characterized at the MP2 and CCSD(T) levels of theory with aug-cc-pVDZ and aug-cc-pVTZ basis sets for n=1-4. Energies of the reactant complex and transitions states are summarized in Tables 3-5. The CCSD(T)/aug-cc-pVTZ energies are displayed in Figure 4. As chlorine is substituted for hydrogen, the complex becomes more strongly bound, until full Cl substitution and then the energy is much less bound. As can be seen in Figure 3, OH^- forms a hydrogen bond with one of the protons on $CH_{(4-n)}Cl_n$, and as Cl is added the proton becomes more acidic and the hydrogen bond becomes stronger. The intrinsic barrier height (energy from the bound complex to the transition state) is higher for proton transfer than for the S_N2 reaction only for the reaction with CH_3Cl. For CH_2Cl_2 and $CHCl_3$, the proton transfer barrier is lower than that for S_N2. This is also consistent with the proton become more acidic as more Cl are substituted.
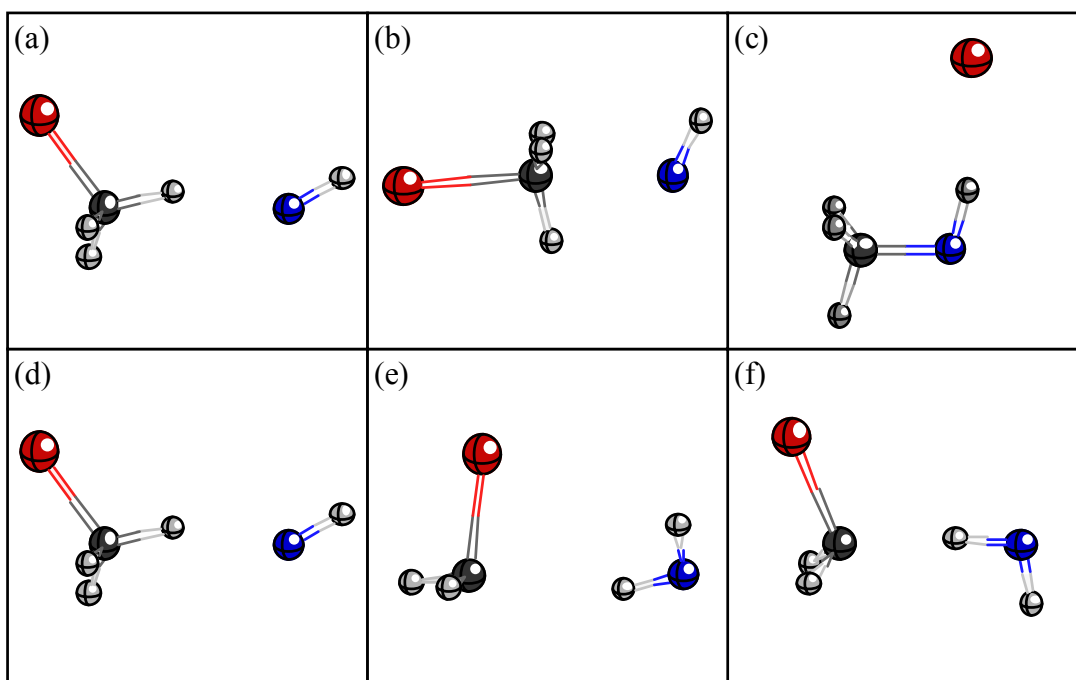
Figure 3. Critical geometries for the S_N2 and proton transfer reactions with CH_3Cl. Reactant complex, transition state, and product complex for the SN2 reaction are shown in parts (a)-(c), respectively, and those for the proton transfer reaction are shown in parts (d)-(f), respectively.
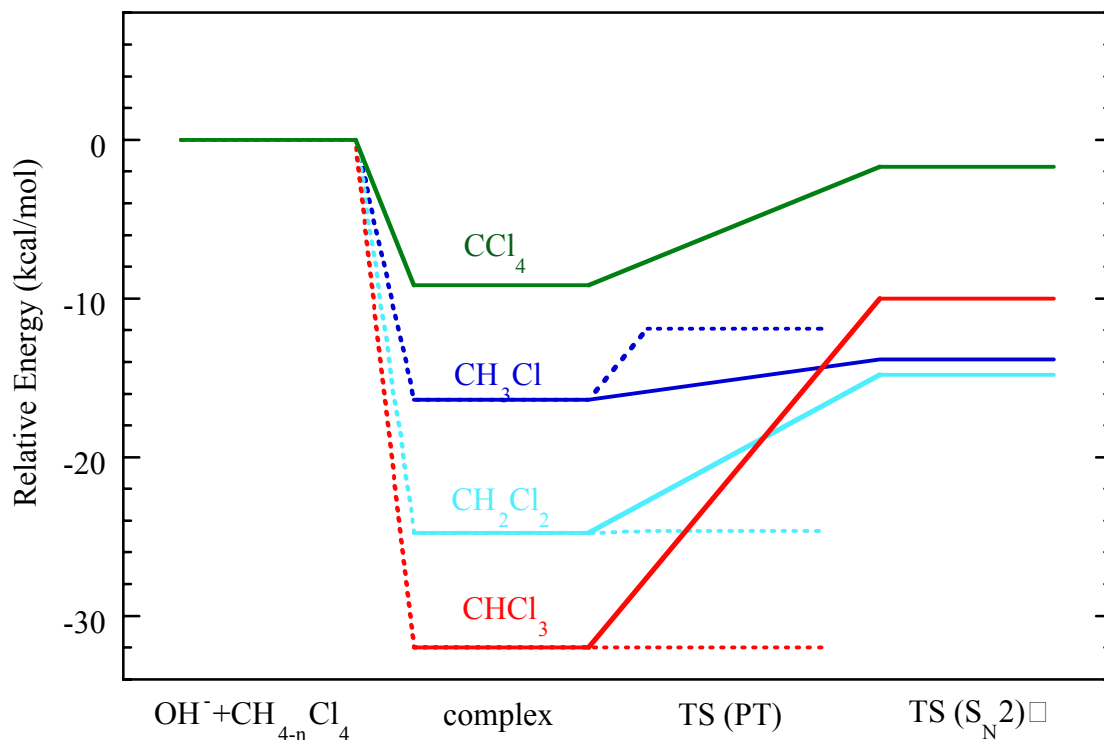
Figure 4. Energies of reactant complexes, $CH_{4-n}Cl_n \cdots OH^-$, and transition states for the proton transfer and S_N2 reactions relative to $CH_{4-n}Cl_n + OH^-$ for n=1-4.

Table 3. Energies of bound complex $OH^- \cdots CH_{(4-n)}Cl_n$ relative to $OH^- + CH_{(4-n)}Cl_n$

	CH_3Cl	CH_2Cl_2	$CHCl_3$	CCl_4
MP2/aVDZ	-16.40	-25.21	-32.1[a]	-8.19
MP2/aVTZ	-15.88	-24.10		-8.76
MP2/aVQZ	-15.78	-24.01		-8.80
MP2/CBS	-15.73	-24.04		-8.77
MP3/aVDZ	-16.91	-25.86		-7.76
MP3/aVTZ	-16.59	-24.97		-8.37
MP3/aVQZ	-16.59	-25.03		-8.44
MP3/CBS	-16.63	-25.18		-8.45
CCSD/aVDZ	-16.30	-24.76		-7.73
CCSD/aVTZ	-15.81	-23.63		-8.17
CCSD(T)/aVDZ	-16.90	-25.88		-8.56
CCSD(T)/aVTZ	-16.39	-24.75		-9.16
(a) results from 6311++G* basis set				

Table 4. Barrier heights for the S_N2 reaction $CH_{4-n}Cl_n \cdots OH^- \rightarrow CH_{4-n}Cl_{n-1}OH \cdots Cl^-$ relative to the energy of the bound complex $OH^- \cdots CH_{(4-n)}Cl_n$.

	CH$_3$Cl	CH$_2$Cl$_2$	CHCl$_3$	CCl$_4$
MP2/aVDZ	2.98	10.55	23.7[a]	7.18
MP2/aVTZ	4.05	11.11		8.37
MP2/aVQZ	4.33	11.32		8.32
MP2/CBS	4.50	11.49		8.13
MP3/aVDZ	3.62	12.35		10.09
MP3/aVTZ	4.54	12.91		11.45
MP3/aVQZ	4.69	13.04		9.63
MP3/CBS	4.76	13.12		7.55
CCSD/aVDZ	2.77	11.04		9.13
CCSD/aVTZ	3.81	11.63		10.61
CCSD(T)/aVDZ	1.61	9.53		6.12
CCSD(T)/aVTZ	2.57	9.96		7.45
(a) results from 6311++G* basis set				

Table 5. Barrier heights for the proton transfer reaction $CH_{4-n}Cl_n \cdots OH^- \rightarrow CH_{3-n}Cl_n \cdots H_2O$ relative to the energy of the bound complex $OH^- \cdots CH_{(4-n)}Cl_n$.

	CH$_3$Cl	CH$_2$Cl$_2$	CHCl$_3$
MP2/aVDZ	5.63	0.30	0[a]
MP2/aVTZ	5.57	0.34	
MP2/aVQZ	5.57	0.32	
MP2/CBS	5.56	0.29	
MP3/aVDZ	3.62	-0.16	
MP3/aVTZ	3.43	-0.12	
MP3/aVQZ	3.42	-0.14	
MP3/CBS	3.42	-0.17	
CCSD/aVDZ	4.95	0.30	
CCSD/aVTZ	4.98	0.42	
CCSD(T)/aVDZ	4.50	0.06	
CCSD(T)/aVTZ	4.48	0.11	
(a) results from 6311++G* basis set			

We have begun studies of the S_N2 and proton transfer reactions with two waters added. The critical geometries are shown in Figure 5 for the reaction with CH_3Cl. The intrinsic barrier (relative the reactant complex) increases dramatically, by about 10 kcal/mol at the MP2/aug-cc-pVDZ level. Further calculations are under way to better characterize this energy.

The minimum energy path was also computed for the S_N2 reaction without waters present and microsolvated with two water molecules. We observe the interesting feature that in going from the saddle point to the reactant complex in the microsolvated reaction, a proton transfer occurs to OH^- from the water hydrogen bonded it, thus forming a new OH^- that is solvated by two waters (see Figure 5).
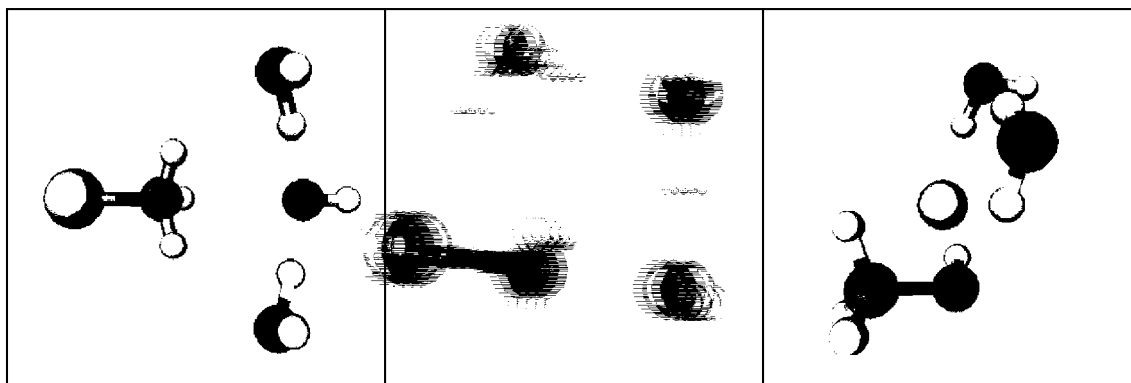

Figure 5. Critical geometries for the $OH^- + CH_3Cl$ S_N2 reaction microsolvated by two water molecules. The reactant complex, transition state, and product complex are shown from left to right.

ONIOM Calculations

We have first examined various level of computational methods in ONIOM calculations to reproduce the structures and energetics obtained with the high level calculation. We have used the structures of $CH_3Cl(H_2O)_n + OH^-(H_2O)_m$, (n+m=1-2) systems calculated with the MP2/aug-cc-pVDZ. We have used the MP2/aug-cc-pVDZ method as a high level calculation for $CH_3Cl + OH^-$ part which is an essential moiety of the solvolytic reaction. The water molecules as solvent are treated as low level. We have examined the HF, BLYP, and B3LYP methods as low level of theory with 6-31+G(d) basis set. When we used the HF and BLYP methods as the low-level calculation, we obtained very different molecular geometries for weakly interacting complexes. Since the hydrogen bonds between water molecule and CH_3 or Cl group are very weak, the molecular interactions between CHCs and water molecules are very flexible throughout the reaction courses. We have found that the best description can be obtained with the combination using the B3LYP method as a low-level calculation.

The relative energy difference between high level MP2 calculations and the ONIOM (MP2:B3LYP) calculations are obtained to be 1.4 kcal/mol in average. When we used the HF and BLYP methods as a low level in the ONIOM calculation, the average error of relative energies is calculated to be 1.9 and 3.6 kcal/mol, respectively. In order to improve the relative energies to describe the potential energy surface, we have carried out the single point

CCSD(T)/aug-cc-pVDZ calculation at the geometries optimized with the ONIOM (MP2/aug-cc-pVDZ:B3LYP/6-31+G(d)) method. This refinement improves the energetics substantially and the relative energies agree with the high level results (CCSD(T)/aug-cc-pVDZ//MP2/aug-cc-pVDZ) within the averaged error by 0.2 kcal/mol in the case of mono-hydrated system.

The advantage of using ONIOM method is clearly demonstrated on the computational time. In the present system, the CPU time of ONIOM calculation is found to be less than 20 % of one required for the high level calculation.

Since the structures obtained the high level calculation do not cover all species on the potential energy surface at the present stage, we need more complete reaction profile even in the di-hydrated systems. The effect of solvation can be taken into account by adding extra water molecules in the system, although various configurations of surrounding water molecules must be considered. This extension will be the second step to explore the energetics of the solvolytic reactions of CHCs in aqueous condition.

In order to explore the effect of substituent effect of chlorine atoms, we have applied the ONIOM method to the system $CH_{4-n}Cl_n + OH^- \rightarrow CH_{4-n}Cl_{n-1}OH + Cl^-$. Comparing the relative energies with the high level MP2 calculations, the ONIOM (MP2:B3LYP) method gives very reasonable energetics for all cases of n=1 - 4 (the average error is within 2 kcal/mol). The single point energies with the CCSD(T)/aug-cc-pVDZ level of theory at the optimized structures of ONIOM method do not improve the energy difference in the case of n=3 and 4.

Although the energy profile is incomplete at the present stage, it is interesting to see the energy barrier of the S_N2 type reactions depending on the number of chlorine atoms as substituents. The lowest energy pathway is found to be in the case of n=2; $CH_2Cl_2 + OH^- \rightarrow CH_2ClOH + Cl^-$. Since the energy barrier is highest in the case of n=4, CCl_4 is concluded to be least reactive in the nucleophilic attack.

QM/MM Calculations of Solvent Effect on Reaction Rates

For the abiotic degradation of $CHCl_3$ in water the favored reaction channel is nucleophilic attack by OH^- or water, followed by decomposition of the resulting anion:

$$HCCl_3 + OH^- \rightarrow CCl_3^- + H_2O \qquad \text{(fast)}$$

$$CCl_3^- \rightarrow Cl_2C: + Cl^- \qquad \text{(slow)}$$

As indicated, the first step is relatively more rapid that the second step. The subsequent pathways are somewhat less clear, although two alternative paths have been suggested. The formation of formyl chloride may either proceed via a unimolecular loss of HCl or through a bimolecular process. The terminal products of the process may be either carbon monoxide or formic acid, as indicated in Figure 6.

16

$$Cl_2C: + H_2O \longrightarrow HC(OH)Cl_2 \xrightarrow{\quad} $$

$$\text{-HCl} \downarrow \qquad \qquad \downarrow OH^-$$

$$\left[\begin{array}{c} O \\ H-\overset{|}{C}-Cl \\ OH \end{array} \right]^{-} \xleftarrow{OH^-} \overset{O}{\underset{Cl \quad H}{C}} \xleftarrow{\quad}$$

$$\downarrow \text{-Cl}^- \qquad \qquad \downarrow OH^-$$

$$HCO_2H \qquad \qquad \underset{Cl}{\overset{O}{C^-}} + H_2O$$

$$\downarrow OH^- \qquad \qquad \downarrow$$

$$HCO_2^- + H_2O \qquad CO + Cl^-$$
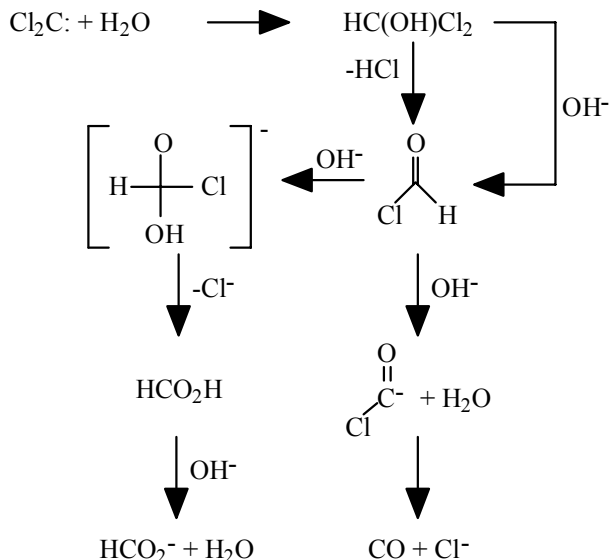
Since the first two steps of the degradation process are well established, and the second reaction is rate limiting, we have decided to investigate the solvent effect on the reaction in water by computing the free energy reaction path using Monte Carlo-QM/MM simulations.

The computational approach features a combination of statistical mechanical Monte Carlo simulation and an ab initio quantum mechanical treatment of the reactive species in water. In particular, CCl_3^- is treated at the ab initio HF/3-21G level throughout the fluid simulations, whereas the water solvent molecules are modeled by Jorgensen's three-point charge TIP3P model. The use of HF/3-21G in these simulations has taken into account the need for computational efficiency since millions of electronic structure calculations are required in the fluid simulation, and a reasonable description of the electronic structure for the decomposition reaction. It is of course desirable to use a larger basis set and perhaps to include electron correlation effects. These issues may be examined in the future. However, it should be emphasized that the results from the Monte Carlo simulations can be decomposed into gas phase energies and solvation free energies. Thus, the free energy profile determined by the combined QM/MM-HF/3-21G simulation can be corrected by higher level gas phase results as follows:

$$\Delta G_{aq}^{H}(R_c) = \Delta G_{aq}^{3-21G}(R_c) + \Delta G_{gas}^{H}(R_c) - \Delta G_{gas}^{3-21G}(R_c)$$

where the superscript H specifies a high-level ab initio theory, $\Delta G_{aq}^{3-21G}(R_c)$ is the potential of mean force computed from QM/MM-HF/3-21G simulations, $\Delta G_{gas}^{H}(R_c)$ and $\Delta G_{gas}^{3-21G}(R_c)$ are gas phase free energies, and R_c is the reaction coordinate for the CCl_3^- decomposition reaction, which is the distance between carbon and the expelled Cl^-.

Table 6 compares the computed energy of reaction at the HF/3-21G//3-21G, B3LYP/6-32+G*//B3LYP/6-31+G* level along with the experimental results, computed from gas-phase heats of formation of the individual species. The HF/3-21G energy is 7.2, and 13.7 kcal/mol more endothermic than experiment and the DFT result.

Table 6. Computed energy of reaction for $CCl_3^- \rightarrow CCl_2 + Cl^-$.

method	ΔE_{rxn} (kcal/mol)
HF/3-21G	43.7
B3LYP/6-31+G*	30.0
exp	36.5

Ab initio QM/MM-Monte Carlo simulations were carried out for a system containing 246 water molecules plus CCl_3^- in a rectangular box of approximately 17.2 x 17.2 x 25.7 Å^3. The isothermal-isobaric ensemble (NPT) was used at 25 °C and 1 atm, along with periodic boundary conditions. A spherical cutoff distance of 8.5 Å, which was limited by the size of the simulation box, was used to evaluate solute-solvent electronic integrals, and solvent-solvent interaction energies. Umbrella sampling was performed for 8 separate simulation windows, covering a range of 1.5 to 6 Å in R_c, to yield the potential of mean force, $W(R_C) = -k_B T \ln P(R_C)$, where $P(R_c)$ is the probability density for finding the reacting system at the reaction coordinate value, R_c. In the simulations, all geometrical parameters are allowed to vary freely during the Monte Carlo simulation. Each simulation was first equilibrated for at least 10^6 configurations, and the results are averaged over the subsequent 2×10^6 configurations. Roughly, one fifth of the Monte Carlo moves required full HF-SCF calculations. Thus, the entire simulation involved about 5 million ab initio HF-SCF calculations. Of course, the rest configurations also have their QM/MM energies computed quantum-mechanically, although the orbitals are not optimized because distant water molecules are moved in the simulation

Shown in Figure 6 is the computed potential of mean force for the CCl_3^- decomposition in water, and the energy profile in the gas phase, both computed at the HF/3-21G level. If a higher level of theory is used, the minimum energy will change accordingly. However, the shape and basic
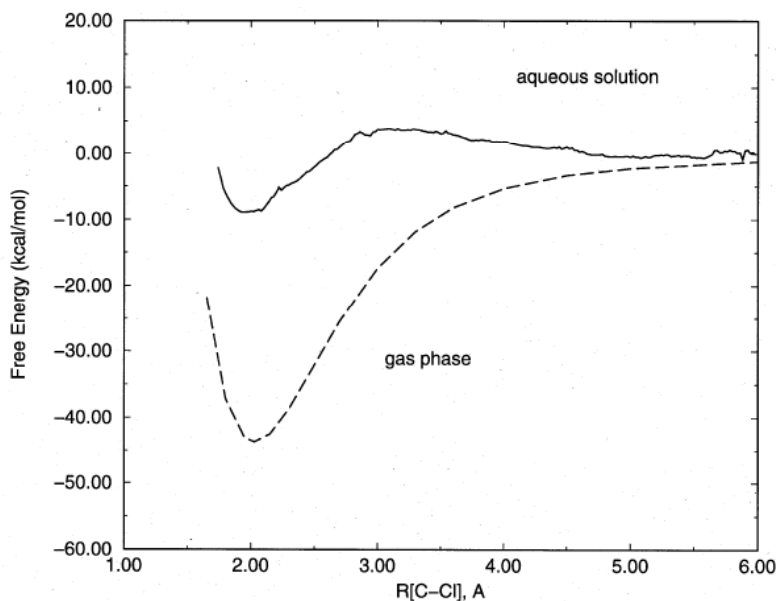

Figure 6. Potential of mean force for CCl_3^- decomposition in water.

features of the reaction profiles should remain. In the gas phase, the energy continuously increases as one of the C-Cl distances is stretched. There is no barrier for recombination of Cl^- and singlet CCl_2. In aqueous solution, the product ion is more stabilized than the CCl_3^- because Cl^- is much better solvated than the larger reactant ion. There is a small solvent-induced barrier of about 3.8 kcal/mol in solution for recombination of Cl^- and CCl_2. The barrier for CCl_3^- dissociation into dichlorocarbene and Cl^- is 12.7 kcal/mol. Thus, the overall solvent effect lowers the barrier for CCl_3^- decomposition by about 30 kcal/mol in water than that in the gas phase. This is consistent with the experimental observation that carbene formation from chloroform is easily achieved in basic solution.

A snap shot of the last configuration corresponding to $R_c = 4.5$ Å is shown in Figure 7. It is interesting to notice that a water molecule forms bridged hydrogen bonds, using its two hydrogens, with the chloride ion and the empty p orbital of dichlorocarbene. Removal of this type of hydrogen-bonding interactions is primarily responsible for the solvent-induced barrier for Cl^- and CCl_2 recombination. In addition, the water-CCl_2 interactions observed here may be relevant for the next reaction step, the insertion of CCl_2 into a H-O bond of a water molecule.
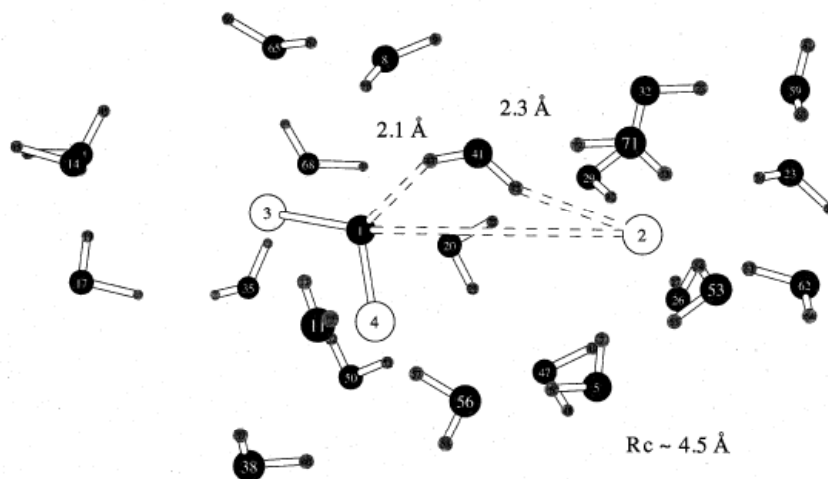

Figure 7. Snap shot of CCl_3^- decomposition in water.

Appendix B — Full Report of Second Year Activities and Accomplishments

Benchmark Ab Initio Electronic Structure Calculations

We continued the benchmark calculations of energies for reactions (R1) and (R2). Preliminary results were reported last year and Tables 1 and 2 provide updated results. The higher level calculations (e.g., CCSD(T)/aug-cc-pVQZ) were complete for all the systems. Differences between computed and experimental reaction energies for the S_N2 and proton transfer reactions of OH^- with $CH_{4-n}Cl_n$ are summarized in Figures 1 and 2. Last year we presented comparisons of the computed and experimental reaction energies only for the reaction with CH_3Cl (n=1). These comparisons have now been extended to the other chlorinated methane molecules.

Values of the extrapolations to the complete basis set (CBS) limit, which are listed in Tables 1 and 2 and plotted in Figures 1 and 2, are obtained as follows. The total energy for each reactant (e.g., OH^-, CH_3Cl, etc.) and product (e.g., Cl^-, CH_3OH, etc.), which are monotonically decreasing functions of the basis set size (x) are extrapolated using the functional form $E_\infty + A (x+1/2)^4 + B (x+1/2)^5$, where x = 2, 3, 4 for the aVDZ, aVTZ, and aVQZ basis sets, respectively. The CBS value for the reaction energies are obtained from the CBS values for each reactant and product. The experimental reaction energy is obtained by subtracting a harmonic estimate of the zero-point vibrational energy from the heat of reaction at 0 K. The heat of reaction is obtained from heats of formation of reactions and products. Error bars on the experimental reaction energy are the sum of the error bars for the heat of reaction and an estimated error bar for the zero-point energies. The major uncertainties in the experimental heats of reaction arise from uncertainties in the heats of formation for the species $CH_{3-n}Cl_nOH$ and $CH_{3-n}Cl_n^-$.

For the S_N2 reaction, the CCSD and CCSD(T) methods are the only methods for which the CBS limit lie within the experimental error bars for all four systems. Except for CCl_4 the CCSD(T) method gives the best estimate for the experimental value. For all four reactions CCSD(T)/CBS is within 2 kcal/mol of the experimental values. For the proton transfer reactions, the experimental error bars are larger than those for the S_N2 reactions, and all methods have CBS values within the experimental error bars. CCSD(T)/CBS gives the best agreement with experiment and is within 1.5 kcal/mol for all 3 reactions.

Figure 3 presents the structures of the bound complexes and transition states for reactions (R1) and (R2) computed at the MP2/aug-cc-pVDZ level of theory. We located the reactant complex (with OH^- hydrogen bonded to one of the protons on the chlorinated methane), the transition state for the S_N2 reaction, the transition state for the PT reaction, and the product complex for the PT reaction (with H_2O hydrogen bonded to the chlorinated methyl anion) at the MP2/aVDZ level of theory. For the reaction with chloroform (n=3) we could not located the reactant complex or a PT transition state at the MP2/aug-cc-pVDZ level of theory, and only the S_N2 transition state and product complex were located. For carbon tetrachloride (n=4) the proton transfer channel is not available and only the reactant complex and S_N2 transition state were located. Energies at these critical geometries have been calculated using MP2, MP3, CCSD, and CCSD(T) with aVDZ, aVTZ, and aVQZ basis sets and are summarized in Tables 3-6. The convergence of the energies (relative to reactant energies) with respect to method and basis set exhibit similar behavior as the reaction energies discussed above. Saddle point energies for the S_N2 reactions (Table 4) show
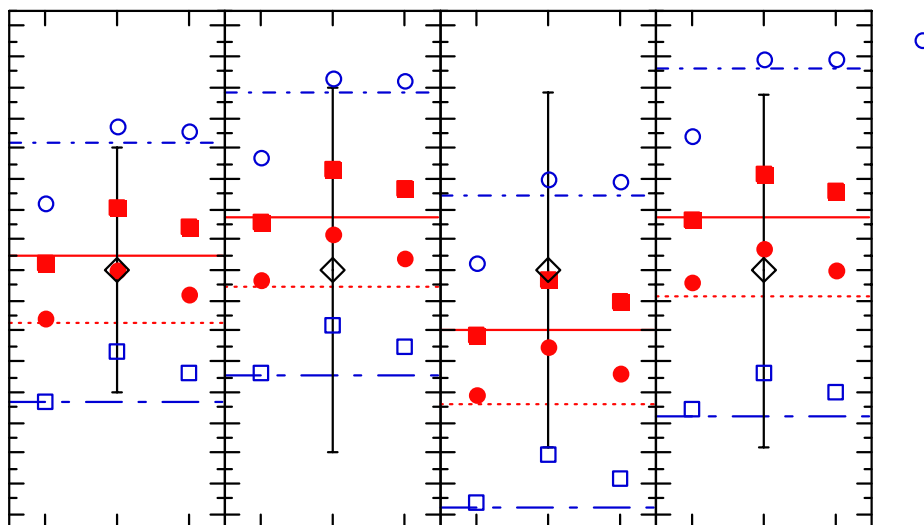
Figure 1. Basis set dependence of differences between computed and experimental reaction energies for the S_N2 reactions $OH^- + CH_{4-n}Cl_n \rightarrow CH_{4-n}Cl_{n-1}OH + Cl^-$. The aug-cc-pVxZ basis sets with $x = D$, T, and Q are denoted aVxZ. The lines are extrapolations to the complete basis set (CBS) limits. The open diamond is set at zero and the error bars depict experimental uncertainties.
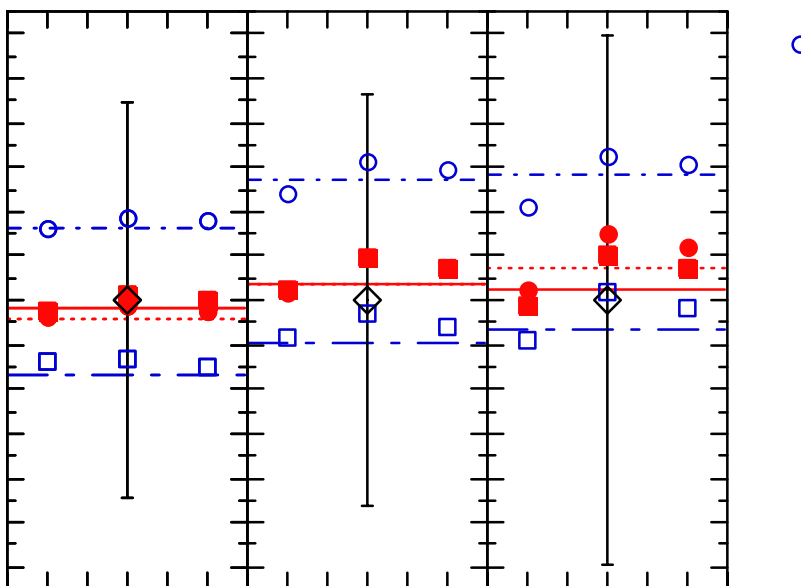

Figure 2. Same as figure 1 except for the differences between computed and experimental reaction energy for the proton transfer reaction $OH^- + CH_{4-n}Cl_n \rightarrow CH_{3-n}Cl_n^- + H_2O$.
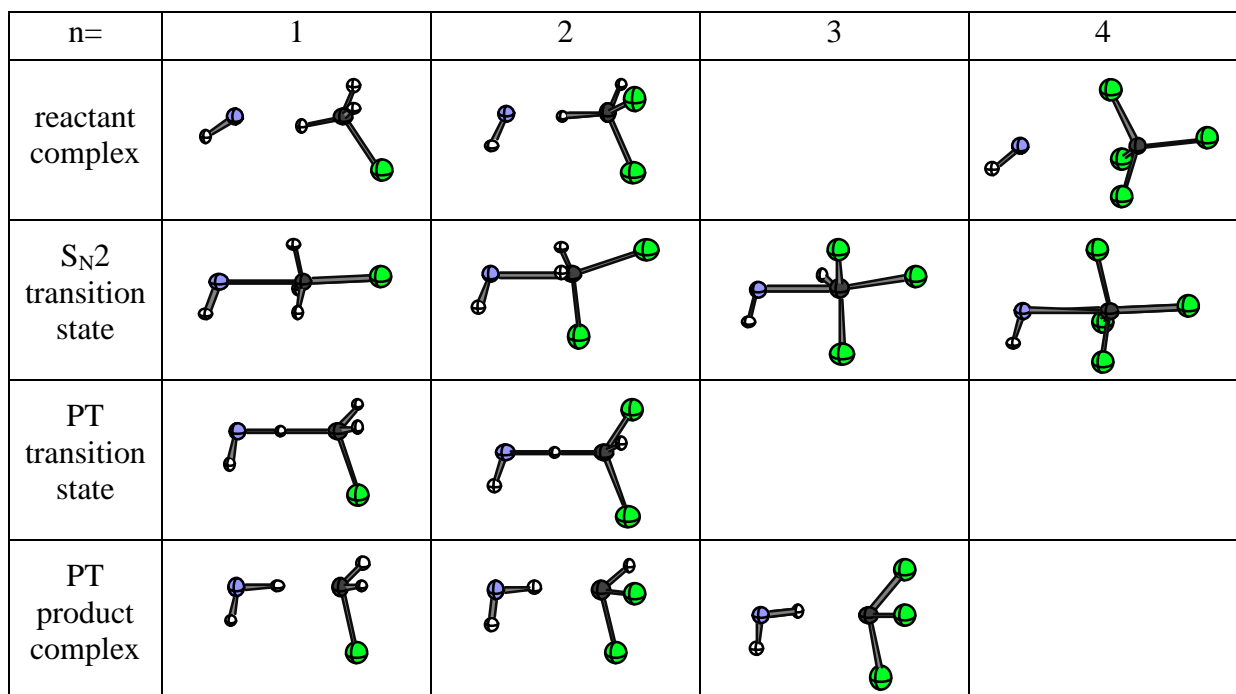
Figure 3. Geometries of reactant complex, S_N2 transition state, proton transfer (PT) transition state, and product complex for the OH^- + $CH_{(4-n)}Cl_n$ reactions for n=1-4. Blank entries indicate that the critical geometries were not located in these cases. Small white, small gray, black, and large green spheres are H, O, C, and Cl atoms, respectively.

slightly larger differences between the CCSD/CBS and CCSD(T)/CBS energies that for the reaction energies in Table 1. Saddle point energies for the PT reactions (Table 6) appear to be better converged with respect to method that the reaction energies shown in Table 2.

The CCSD(T)/CBS energies are displayed in Figure 4. As chlorine is substituted for hydrogen, the complex becomes more strongly bound, until full Cl substitution and then the energy is much less bound. As can be seen in Figure 3, OH^- forms a hydrogen bond with one of the protons on $CH_{(4-n)}Cl_n$, and as Cl is added the proton becomes more acidic and the hydrogen bond becomes stronger. The intrinsic barrier height (energy from the bound complex to the transition state) is higher for proton transfer than for the S_N2 reaction only for the reaction with CH_3Cl. For CH_2Cl_2 and $CHCl_3$, the proton transfer barrier is lower than that for S_N2. This is also consistent with the proton become more acidic as more Cl atoms are substituted.

We have continued studies of the microsolvation of the S_N2 and proton transfer reactions. The effects of one and two water molecules on the reaction energetics for the S_N2 reaction of OH= with CH_3Cl are shown in Figure 5. The OH^- anion has a large solvation energy and binds water molecules more strongly than the other species (e.g., CH_3Cl, CH_3OH, and Cl^-). Therefore the decrease in solvation energy in forming the products increases the product energy relative to the reactant energy. Forming the complex of OH^- with CH_3Cl also decreases the solvation energy, although to a lesser degree, so the changes in the relative energies of the reactant complexes are smaller. The excess charge, which is largely localized on OH in the reactant complex, is more delocalized at the saddle point for the S_N2 reaction as Cl^- is being formed. Thus the solvation energy of the saddle point is significantly decreased relative to reactants, thereby increasing the
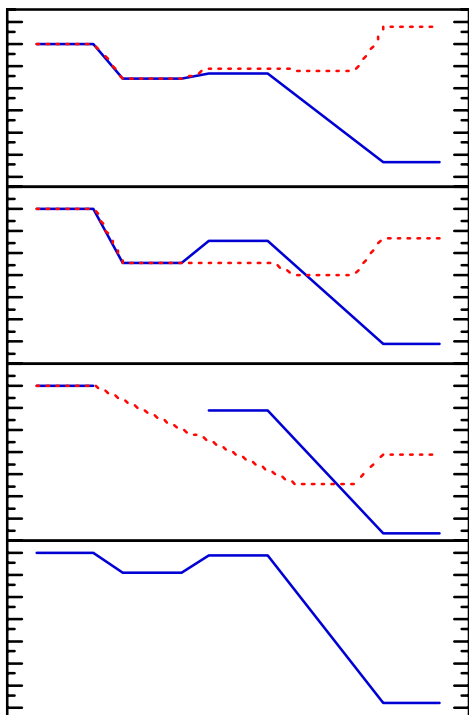
Figure 4. Energies (calculated at the CCSD(T)/CBS level of theory) of reactant complexes, transition states, product complexes and products relative to the reactant energies for the OH$^-$ + CH$_{(4-n)}$Cl$_n$ reactions. Parts (a) - (d) are for n=1-4, respectively. The zero of energy in each part is the reactant energy. Solid lines are for the S$_N$2 reactions and dashed lines are for the proton transfer reactions. For n=1 and 2, the reactant complexes are the same for the S$_N$2

Figure 5. Energies (calculated at the MP2/aVDZ level of theory) of reactant complexes, transition states, product complexes and products relative to the reactant energies for the S$_N$2 reaction OH$^-$(H$_2$O)$_m$ + CH$_3$Cl with m=0 (solid line labeled gas phase), n=1 (long dashed line labeled one water) and n=2 (short dashed line labeled two waters).

saddle point energy upon solvation by almost 10 kcal/mol. The product complex corresponds to Cl$^-$ solvated by methanol and water molecules, which again has a solvation energy that is decreased relative to the solvation of the reactants.

We have calculated the minimum energy path (MEP) for the reaction OH$^-$(H$_2$O)$_2$…CH$_3$Cl $\rightarrow$ CH$_3$OH…Cl$^-$(H$_2$O)$_2$. The energy profile for this reaction is compared with the gas-phase (no solvation by water molecules) energy profile is Figure 6. This figure also shows snapshots of geometries along the MEP for the microsolvated reaction. Note that near the reactant complex (left side of the figure) OH$^-$ is symmetrically solvated by two water molecules and is approaching one of the protons on CH$_3$Cl. Moving towards the saddle point at s=0, there is a proton transfer between OH$^-$ and one of the water molecules to form a new OH$^-$ molecule which is now asymmetrically solvated, but properly aligned for the S$_N$2 process (i.e., the O - C - Cl angle is near collinear. We see that water molecules can be directly involved in the S$_N$2 reaction process and that some water molecules will need to be explicitly treated in the electronic structure calculations of approximate treatments of bulk solvation such as QM/MM or continuum solvation approaches.

Figure 6. Energy (calculated at the MP2/aVDZ level of theory) along the minimum energy path for the process $OH^-(H_2O)_n \ldots CH_3Cl \rightarrow CH_3OH \ldots Cl^-(H_2O)_n$, for n=0 (solid line labeled gas phase) and n=2 (dashed line labeled microsolvated).

Similar studies of the effects of microsolvation were carried out for the proton transfer reaction of $OH^=$ with CH_3Cl. As shown in Figure 4(a), the intrinsic barrier for the proton transfer reaction in the gas phase is very small, 2.9, 4.5, and 3.0 kcal/mol at the CCSD(T)/CBS, MP2/CBS, and MP2/aVDZ levels of theory, respectively. Upon solvation with two water molecules, we could no longer find the PT product complex or transition state. Figure 7 presents MP2/aVDZ energies at the reactant complex, saddle point, product complex and products, all relative to the reactant energies, for the gas-phase critical geometries. The relative energy at the critical geometry for the reactant complex is also shown for the microsolvated reaction. The energies for the microsolvated saddle point and product complex are obtained by constraining the OH^--CH_3Cl complex to the gas-phase critical geometries and optimizing the geometries of the two water molecules. These calculations
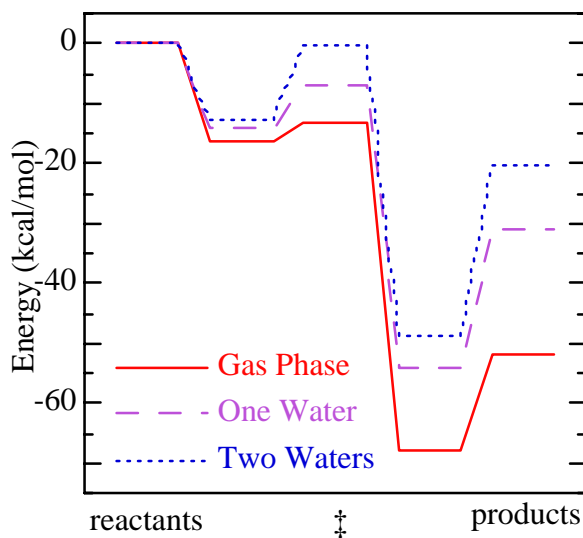

Figure 7. Energies (calculated at the MP2/aVDZ level of theory) of reactant complexes, transition states, product complexes and products relative to the reactant energies for the PT reaction $OH^-(H_2O)_m + CH_3Cl$ with m=0 (solid line labeled gas phase) and n=2 (dashed line labeled microsolvated).

indicate that the energy from the products to the reactant complex is monotonically downhill in

energy. This conjecture was confirmed by starting at a geometry in the asymptotic product channel for the PT reaction corresponding to $(H_2O)_3$ separated from CH_2Cl^- and following the minimum energy path back towards the complex region. Energies along this reaction path (relative to reactants) are shown in Figure 8. This figure also shows snapshots of geometries along the MEP. The shoulder in the energy occurs near where the proton hops between the water trimer and CH_2Cl^-, indicating that this feature in the energy profile is a remnant of the small barrier in the gas-phase reaction. In this case microsolvation not only affects the energetics of the reaction, it alters gross features on the potential energy surface.

We have initiated studies of the reactions $OH^- + CH_2CH_{(2-n)}Cl_n$ at the MP2/aVDZ level of theory. For these gas-phase reactions OH^- abstracts a proton from the C1 position (carbon with no chlorine atoms) with no barrier to the reaction. These systems have small barriers to the elimination of Cl^- to form acetylene and a hydrated chloride ion.

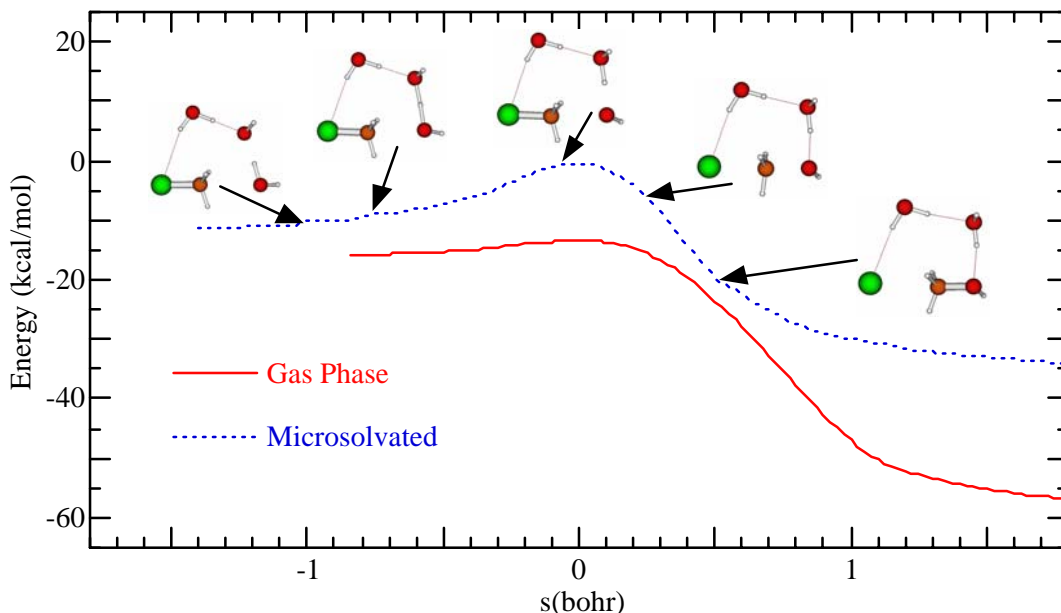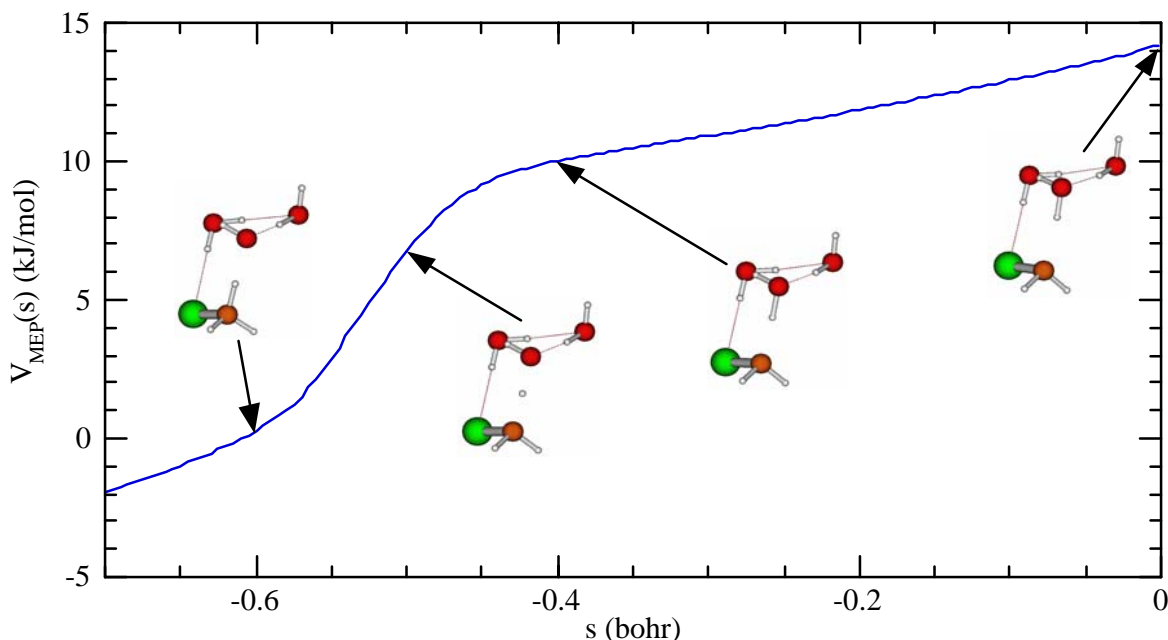**Figure 8**. Energy (calculated at the MP2/aVDZ level of theory) along the minimum energy path for the process $OH^-(H_2O)_2\ldots CH_3Cl \rightarrow CH_2Cl^- + (H_2O)_3$. The zero of energy is the equilibrium reactant geometry for $OH^-(H_2O)_2 + CH_3Cl$.

QM/MM Simulations

Treatment of the effects of bulk solvation on the reaction energetics is being treated using hybrid quantum mechanical / molecular mechanics (QM/MM) methods and with continuum solvation approaches. Comparison of the QM/MM and continuum solvation requires computing energetics along the reaction path in which averages are performed over solvent configurations. Solvent averaging is implicit in the continuum solvation approaches, but averaging over solvent configurations needs to be carried out explicitly in the QM/MM method to yet an effective potential for the reacting species, the so-called potential of mean force (PMF). In the previous year we initiated efforts to develop efficient procedures to calculate the PMF.

The simplest type of mixed quantum mechanical / molecular mechanics approach is to obtain the geometries and energies along a gas-phase minimum energy path (MEP) using electronic structure theory, and then for each geometry along the gas-phase MEP compute a solvation energy using molecular mechanics. In this approach the solvent-solute potential is a combination of Lennard-Jones and coulombic interactions, where the charges on the solute are obtained by fitting the computed electrostatic potential. We denote this approach QM+MM. This approach has been applied to the S_N2 reaction of $OH^- + CH_3Cl$ with 20 water molecules. The water-water interactions are modeled using the TIP3P model. The gas-phase reaction path is the MEP obtained at the MP2/aVDZ level of theory. Note that the solute charges used in the solute-solvent interaction varied along the path. Runs used 128 processors with 500,00 equilibration steps and 500,000 sampling steps per node for a total of 64 million Monte Carlo steps. Each of the 128 runs started with a different random configuration of waters. The energy profile in Figure 9 is the sum of the HF/6-31G* energies along the MEP and the solvation energy obtained by the PMF simulation.

At the next level of complexity, the electronic structure calculations for the solute molecule at a fixed geometry is recomputed for each set of solvent geometries, where the coupling of the charges on the solvent molecules to the electron distribution on the solute is included explicitly in the electronic structure calculations. This approach is what is traditionally denoted QM/MM. This approach has also been applied to the S_N2 reaction of $OH^- + CH_3Cl$ with 20 water molecules. To allow direct comparison with the QM+MM approach we used the same solute geometries along the gas-phase MEP, and used HF/6-31G* for the solute and TIP3P for the water molecules. Calculations of millions of electronic structure calculations at the relatively low level of HF/6-31G* are currently not feasible, even with the power of the MPP. In order to enable the QM/MM calculations, we have developed new sampling techniques that should allow estimates of the QM/MM energies to be obtained using far fewer electronic structure calculations. In this approach, solvent configurations from the QM+MM calculations are used as a reference system, solvent geometries from the QM+MM calculation are stored, and QM/MM calculations are performed for solvent geometries randomly sampled from those stored. The results shown in Figure 9 are from runs of 64 processors with 500,000 MM equilibration steps, 500,000 MM sampling steps and 100 QM averaging steps per node.
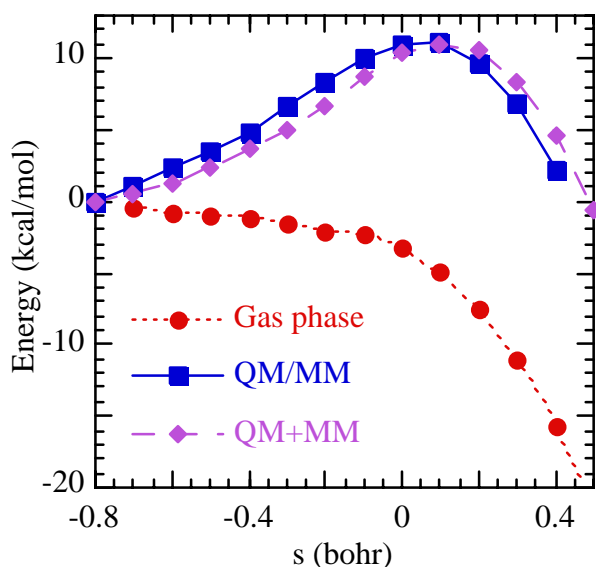
Figure 9. Energy as a function of reaction coordinate for the process OH^- $(H_2O)_n...CH_3Cl \rightarrow CH_3OH...Cl^-(H_2O)_n$, for n=0 and 20. Electronic structure calculations are carried out at the HF/6-31G* level of theory at geometries along the MP2/aVDZ minimum energy path. The gas-phase results (n=0) are indicated by solid circles connected by a short dashed line. Calculations for n=20 are the QM+MM method (diamonds connected by a long dashed line) and the QM/MM

Appendix C — Full Report of Third Year Activities and Accomplishments

Benchmark Ab Initio Electronic Structure Calculation

During the third year of this project significant progress was made in completing the benchmark calculations for microsolvated versions of S_N2 and proton transfer reactions of OH^- with $CH_{4-n}Cl_n$

$$OH^-(H_2O)_m + CH_{4-n}Cl_n \rightarrow CH_{4-n}Cl_{n-1}OH(H_2O)_{m-m'} + Cl^-(H_2O)_{m'} \qquad \text{(R3)}$$

$$OH^-(H_2O)_m + CH_{4-n}Cl_n \rightarrow H_2O(H_2O)_{m-m'} + CH_{3-n}Cl_n^-(H_2O)_{m'} \qquad \text{(R4)}$$

Our efforts focused on the reactions of CH_3Cl and CH_2Cl_2 (e.g., $n = 1\text{-}2$) and $m = 0\text{-}2$. Using the same protocol established for the reaction with no solvation by water molecules, critical geometries were optimized at the MP2/aug-cc-pVDZ level of theory and single point calculations were performed at these geometries using MP2, MP3, CCSD, and CCSD(T) with complete basis set (CBS) estimates obtained using the aug-cc-pVxZ basis sets with x=2,3,4. In addition, we used a two-point extrapolation formula[1]

$$E_\infty^{\text{CCSD(T)}} \approx E_\infty^{\text{CCSD(T)}\|MP3} = E_3^{\text{CCSD(T)}} + \gamma^{MP3}\left(E_3^{\text{CCSD(T)}} - E_2^{\text{CCSD(T)}}\right)$$

where E_∞^Y is the complete basis set limit to the electronic energy for method Y, E_x^Y is the electronic energy for method Y with the aug-cc-pVxZ basis set and

$$\gamma^{MP3} = \left(E_\infty^{MP3} - E_3^{MP3}\right) / \left(E_3^{MP3} - E_2^{MP3}\right)$$

We introduced the notation CCSD(T)‖MP3 to denote that the CBS extrapolation of CCSD(T) is assumed to converge at the same rate as theory MP3 and can be approximated by the simple 2-point extrapolation formula given above.

Results for the microsolvated reactions are summarized in Tables 1-3. For the reaction energies we report only the results for $m' = 0$, in which the solvating water molecules stay with the OH moiety. For the energies of reactions (R3), moving one water molecule from the alcohol $CH_{4-n}Cl_{n-1}OH$ to Cl^- makes the reaction more exoergic by 9-10 kcal/mol for $m = 0$ but only about 4 kcal/mol for $m = 1$. The convergence of the reaction energy with respect to basis set and level of theory is almost identical to the convergence seen for $m' = 0$, so we do not report those values for the solvated Cl^- products. For the energies of reactions (R4), the $CH_{3-n}Cl_n^-(H_2O)$ species with $n = 1$ and 2 tend to be unstable with respect to adding one or two water molecules, since the solvation energy of OH^- is larger than for the carbanion. Therefore, we only report the $m' = 0$ results for these reactions also.

Table 1-4 show that the good convergence of the energies with respect to basis set and level of theory, which we observed for the nonsolvated reactions ($m = 0$), is repeated for the microsolvated reactions with $m = 1$ and 2. For some of the systems we did not perform the CCSD

Table 1. Reaction energies (in kcal/mol) for the S_N2 reaction $OH^-(H_2O)_m + CH_{4-n}Cl_n \rightarrow$ $CH_{4-n}Cl_{n-1}OH(H_2O)_m + Cl^-$, for $n = 1$ and 2 and m = 0-2. The basis sets aVxZ denote the aug-cc-pVxZ basis sets, CBS denotes extrapolation to the complete basis set limit, and ZPE denotes a harmonic approximation to the zero point energy.

	n = 1			*n* = 2		
	m = 0	*m* = 1	*m* = 2	*m* = 0	*m* = 1	*m* = 2
MP2/aVDZ	-51.7	-31.2	-20.2	-59.2	-37.5	-27.4
MP2/aVTZ	-49.2	-37.1	-25.6	-66.3	-34.2	-24.0
MP2/aVQZ	-49.3	-35.0	-23.6	-63.2	-34.5	-24.2
MP2/CBS	-49.5	-32.9	-21.7	-61.4	-34.7	-24.5
MP3/aVDZ	-58.2	-28.0	-17.0	-56.6	-44.2	-33.4
MP3/aVTZ	-56.6	-34.7	-23.0	-64.8	-41.8	-30.7
MP3/aVQZ	-57.3	-32.8	-21.2	-61.7	-42.5	-31.4
MP3/CBS	-57.8	-30.4	-19.1	-59.6	-43.1	-32.0
CCSD/aVDZ	-55.5	-28.2	-17.3	-56.7	-41.8	-31.1
CCSD/aVTZ	-53.9	-35.3	-23.7	-65.5	-39.5	-28.5
CCSD/aVQZ	-54.7	-33.5		-62.5	-40.3	
CCSD/CBS	-55.2	-31.1		-60.3	-41.0	
CCSD(T)/aVDZ	-53.6	-28.5	-17.7	-56.9	-39.6	-29.3
CCSD(T)/aVTZ	-51.8	-35.9	-24.3	-66.0	-37.0	-26.5
CCSD(T)/aVQZ	-52.5	-34.2		-63.1	-37.8	
CCSD(T)/CBS	-53.0	-31.7		-60.8	-38.4	
CCSD(T)|MP3	-53.0	-31.7	-20.6	-60.9	-38.4	-27.9

Table 2. Reaction energetics (in kcal/mol) for the PT reaction of $OH^-(H_2O)_m + CH_{4-n}Cl_n \rightarrow CH_{3-n}Cl_{n-1}^-(H_2O)_m + Cl^-$, for $n = 1$ and 2 and $m = 0$-2. The basis sets aVxZ denote the aug-cc-pVxZ basis sets, CBS denotes extrapolation to the complete basis set limit, and ZPE denotes a harmonic approximation to the zero point energy.

	$n = 1$			$n = 2$		
	$m = 0$	$m = 1$	$m = 2$	$m = 0$	$m = 1$	$m = 2$
MP2/aVDZ	11.0	32.5	43.4	-9.4	12.1	23.0
MP2/aVTZ	11.6	33.5	38.3	-15.9	14.0	24.9
MP2/aVQZ	11.4	33.2	39.6	-13.8	13.6	24.4
MP2/CBS	11.2	32.9	40.1	-13.7	13.2	24.0
MP3/aVDZ	5.0	26.7	44.4	-8.0	5.9	17.4
MP3/aVTZ	5.2	27.6	39.2	-14.8	7.7	19.3
MP3/aVQZ	4.8	27.3	40.7	-12.3	7.0	18.6
MP3/CBS	4.6	27.0	41.3	-12.2	6.6	18.1
CCSD/aVDZ	7.0	28.2	44.0	-8.3	7.3	18.7
CCSD/aVTZ	7.6	29.3	38.8	-15.4	9.4	20.9
CCSD/aVQZ	7.3	28.9	40.3	-12.8	8.8	20.3
CCSD/CBS	7.1	28.6	40.9	-12.7	8.4	19.8
CCSD(T)/aVDZ	7.4	29.6	43.7	-8.5	9.0	19.0
CCSD(T)/aVTZ	8.0	29.6	38.5	-15.8	8.8	21.1
CCSD(T)/aVQZ	7.8	29.5	40.0	-13.2	8.7	20.4
CCSD(T)/CBS	7.6	29.5	40.6	-13.1	8.8	19.9
CCSD(T)|MP3	7.6	29.6	40.7	-13.2	8.8	19.9

Table 3. Energetics (in kcal/mol) of bound complex $OH^-(H_2O)_m \cdots CH_{(4-n)}Cl_n$ relative to OH^- $(H_2O)_m + CH_{4-n}Cl_n$, for $n = 1$ and 2 and $m = 0\text{-}2$.

	$n = 1$			$n = 2$		
	$m = 0$	$m = 1$	$m = 2$	$m = 0$	$m = 1$	$m = 2$
MP2/aVDZ	-16.4	-14.3	-12.9	-25.2	-20.7	-12.9
MP2/aVTZ	-15.9	-13.6	-11.9	-24.1	-19.5	-11.9
MP2/aVQZ	-15.8	-13.4	-11.8	-24.0	-19.3	-11.8
MP2/CBS	-15.7	-13.4	-11.7	-24.0	-19.3	-11.7
MP3/aVDZ	-16.9	-14.5	-12.9	-25.9	-20.9	-12.9
MP3/aVTZ	-16.6	-13.8	-11.9	-25.0	-19.7	-11.9
MP3/aVQZ	-16.6	-13.7	-11.8	-25.0	-19.6	-11.8
MP3/CBS	-16.6	-13.6	-11.8	-25.1	-19.6	-11.8
CCSD/aVDZ	-16.3	-14.1	-12.6	-24.8	-20.3	-12.6
CCSD/aVTZ	-15.8	-13.4	-11.6	-23.6	-19.0	-11.6
CCSD/aVQZ	-15.7			-23.6		
CCSD/CBS	-15.7			-23.6		
CCSD(T)/aVDZ	-16.9	-14.7	-13.3	-25.9	-21.2	-13.3
CCSD(T)/aVTZ	-16.4	-13.9	-12.2	-24.7	-19.8	-12.2
CCSD(T)/aVQZ	-16.3			-24.7		
CCSD(T)/CBS	-16.2			-24.7		
CCSD(T)|MP3	-16.3	-13.7	-12.1	-24.8	-19.7	-12.1

Table 4. Energetics (in kcal/mol) of saddle points for the S_N2 reactions relative to OH⁻ $(H_2O)_m + CH_{4-n}Cl_n$, for $n = 1$ and 2 and $m = 0\text{-}2$.

	$n = 1$			$n = 2$		
	$m = 0$	$m = 1$	$m = 2$	$m = 0$	$m = 1$	$m = 2$
MP2/aVDZ	-13.4	-6.9	-0.3	-14.7	-7.1	1.8
MP2/aVTZ	-11.8	-4.6	2.3	-13.0	-4.5	4.4
MP2/aVQZ	-11.5	-4.3	2.9	-12.7	-4.2	4.6
MP2/CBS	-11.3	-4.1	3.2	-12.5	-4.1	4.6
MP3/aVDZ	-13.3	-6.7	0.8	-13.5	-5.8	3.8
MP3/aVTZ	-12.0	-4.6	3.3	-12.1	-3.2	6.5
MP3/aVQZ	-11.9	-4.5	3.6	-12.0	-3.1	6.6
MP3/CBS	-11.8	-4.4	3.6	-12.0	-3.1	6.5
CCSD/aVDZ	-13.5	-7.2	0.1	-13.7	-6.2	3.2
CCSD/aVTZ	-12.0	-4.9	2.9	-12.0	-3.5	6.1
CCSD/aVQZ	-11.7			-11.8		
CCSD/CBS	-11.6			-11.7		
CCSD(T)/aVDZ	-15.3	-8.9	-2.2	-16.4	-8.8	0.3
CCSD(T)/aVTZ	-13.8	-6.7	0.5	-14.8	-6.3	2.9
CCSD(T)/aVQZ	-13.5			-14.6		
CCSD(T)/CBS	-13.3			-14.5		
CCSD(T)|MP3	-13.5	-6.5	0.8	-14.7	-6.2	2.9

and CCSD(T) calculations with the largest basis set (aVQZ). The excellent agreement of the CCSD(T)|MP3 results with those for CCSD(T)/CBS, for those systems for which we did complete calculations, indicates that this 2-point approximation should give an excellent approximation to the CCSD(T)/CBS energies in all cases.

Table 5 and Figure 1 summarize the CCSD(T)|MP3 results for the energies of complexes, saddle points and reaction, relative to the reactant energies, for the OH⁻ $(H_2O)_m + CH_{(4-n)}Cl_n$ reactions with $n = 1$ and 2 and $m = 0\text{-}2$. Note that there are also complexes on the product side of the saddle points for the S_N2 reactions, which are not listed in Table 5 or shown in Figure 1. At the MP2/aVDZ level of theory they are lower in energy that the S_N2 products by 16.3, 22.8, and 28.5 kcal/mol for the reaction with $n = 1$ and $m = 0$, 1, and 2, respectively. This part of the potential energy surface does not affect the computed reaction rates, so we have not studied these complexes in greater detail at this time.

Table 5. CCSD(T)|MP3//MP2/aug-cc-pVDZ Energies of Reaction, Complexes, and Saddle Points Relative to Reactants OH^- $(H_2O)_m$+ $CH_{(4-n)}Cl_n$ for $n = 1$ and 2 and $m = 0\text{-}2$.

	$n = 1$			$n = 2$		
	$m = 0$	$m = 1$	$m = 2$	$m = 0$	$m = 1$	$m = 2$
Reactant complex	-16.3	-13.7	-12.1	-24.8	-19.7	-17.8
S_N2 saddle point	-13.5	-6.5	0.8	-14.7	-6.2	2.9
S_N2 Products	-53.0	-31.7[a]	-20.6[a]	-60.9	-38.4[a]	-27.9[a]
		-40.9[a]	-24.6[a]		-48.7[a]	-31.3[a]
PT complex	-12.7	[b]	[b]	-29.9	[b]	
PT saddle point	-11.8	[b]	[b]	-24.7	[b]	
PT Products	7.6	29.6	40.7	-13.2	8.8	19.9

(a) Top entry is for product with $m' = 0$, bottom entry is for $m' = 1$.
(b) Proton transfer complexes were not located for these reactions.

We can see a few general trends from Figure 1. First, since the hydration energy of OH^- is greater than any of the product species, the reaction energies for both the S_N2 and PT reactions increases upon solvation. At the CCSD(T)|MP3 level of theory, the hydration energy for OH^-, Cl^-, CH_2Cl^-, $CHCl_2^-$, H_2O, CH_3OH, CH_2ClOH, CH_3Cl, and CH_2Cl_2 are 27.0, 14.9, 20.4, 16.8, 5.0, 5.7, 4.6, 3.8, and 4.0 kcal/mol, respectively. The changes in reaction energies for reactions (R3) and (R4) in going from $m = 0$ to $m = 1$ with $m' = 0$ are all 22.1±0.6 kcal/mol. This energy change is given as the difference in the solvation energy of OH^- and the water or alcohol molecule in products. The energy differences are all close because water and the two alcohol molecules have hydration energies with the range 4.6 – 5.7 kcal/mol. Similarly, the changes in reaction energies for reactions (R3) and (R4) upon solvation by two water molecule (to give $m = 2$ and $m' = 0$) are 10.8±0.3 kcal/mol. Second, the energies of the reactant complexes are shifted by 5.1 kcal/mol or less upon solvation by one water molecule and by 7.0 kcal/mol or less upon solvation by two water molecules. The shifts can be understood in terms of the differential solvation energies for reactants and the complexes. The OH^- anion forms a fairly strong complex with the $CH_{4-n}Cl_n$ molecules, with OH^- hydrogen bonded with one of the protons on $CH_{4-n}Cl$. The CCSD(T)|MP3 energies of these complexes relative to OH^- + $CH_{4-n}Cl$ are -16.3 and -24.8 kcal/mol for $n = 1$ and 2, respectively. When the complex is formed with a hydrated OH^- anion, the fairly strong binding to $CH_{4-n}Cl$ weakens the $OH^-...H_2O$ energy by about 2.6 and 5.1 kcal/mol for CH_3Cl and CH_2Cl_2, respectively. The strong binding of OH^- to CH_2Cl_2 compared to CH_3Cl gives rise to larger changes in the differential solvation energy for the former and therefore larger shifts with solvation in the energies of the reactant complexes for $n = 2$. Third, the energies of the S_N2 saddle point, relative to reactants, have significantly larger shifts upon hydration than the reactant complexes. Formation of the S_N2 saddle point perturbs the OH^- – water interaction even more so that the hydration energy of the saddle point is 7.0 and 8.5 kcal/mol weaker than for OH^- for $n = 1$ and 2, respectively.

Reaction rates constants were calculated using variational transition state theory (VTST) and the accurate energetics benchmarked above. The minimum energy pathway was constructed by

following the path of steepest descent in a mass-weighted coordinate system from the saddle point into the reactant complex and into products, and from the asymptotic reactants into the reactant complex. The energy and its first and second derivatives (gradients and Hessian) along the MEP were computed at the MP2/aVDZ level of theory and the energies were corrected by evaluation at the CCSD(T)|MP3 level at several points along the MEP. From Figure 5 it is apparent that the dynamical bottleneck for some of the reactions occur in the asymptotic reactant region where the energy along the MEP is the highest. Phase-space-integral-based VTST (PSI-VTST), which is appropriate for treating loose transition states found in barrierless association reactions and unimolecular reactions is used to compute rate constants for transition-state dividing surfaces (bottlenecks) in the entrance channel. For bottlenecks near the saddle point of the reaction we used canonical variation theory (CVT) as implemented in the POLYRATE program. In these calculation we employ direct dynamics techniques in which the energies, gradients, and Hessians from electronic structure calculations are used directly in the rate constant calculation without fitting them first to an analytical functional form. For variational transition states with large center-of-mass separations, the potential along the MEP is dominated by electrostatic interactions (*e.g.*, charge-dipole interactions). In these cases, we found that the potential energy surface could be adequately represented using a multipole expansion for the potential. In the electrostatic model $O\tilde{H}$ and $CH_{(4-n)}Cl_n$ are treated as rigid molecules with charge distributions characterized by total charge, dipole moment, quadrupole moment, etc., and polarizabilities.

Rate constants for the S_N2 reactions are presented in Tables 6 and 7, where they are compared with the experimental values of Staneke et al.[3] and Bohme and Raksit.[4] For the reactions with $n = 1$-3, the PSI-VTST rate constants, which have the transition-state dividing surfaces in the asymptotic entrance channel, are lower than the CVT rate constants, which have the dividing surfaces near the saddle point, indicating that the dynamical bottlenecks for these reactions are in the asymptotic reactant regions of the potential energy surfaces. For the CCl_4 reaction the

Table 6. Bimolecular Rate Constants (Units of cm^3 molecule^{-1} s^{-1}) for the Reactions of OH^- with $CH_{(4-n)}Cl_n$ (n = 1–4) at 300 K

n	k^{CVT}	$k^{PSI\text{-}VTST}$	$k^{exp\ a}$
1	7.9×10^{-4}	3.9×10^{-9}	1.5×10^{-9}
2	9.0×10^{-3}	3.6×10^{-9}	2.1×10^{-9}
3	1.8×10^{-5}	3.1×10^{-9}	2.6×10^{-9}
4	1.3×10^{-12}	5.5×10^{-9}	2.2×10^{-10}

(a) Rate constants (summed over all product channels) from the experiments of Staneke *et al.*

Table 7. Bimolecular Rate Constants (Units of cm^3 molecule^{-1} s^{-1}) for the Reactions of $OH^-(H_2O)_m$ with CH_3Cl (m = 0-2) at 300 K

m	k^{CVT}	$k^{PSI\text{-}VTST}$	$k^{exp\ a}$
0	7.9×10^{-4}	3.9×10^{-9}	1.5×10^{-9}
1	9.6×10^{-10}	3.1×10^{-9}	6.0×10^{-10}
2	5.8×10^{-16}	2.9×10^{-9}	$<2.0 \times 10^{-12}$

(a) Rate constants for S_N2 reaction from the experiments of Bohme *et al.*

[3] P. O. Staneke, G. Groothuis, S. Ingemann, N. M. M. Nibbering, J. Phys. Org. Chem. **9**, 471 (1996).

[4] D. K. Bohme, A. B. Raksit, J. Am. Chem. Soc. **106**, 3447 (1984).

dynamical bottleneck is near the saddle point and the CVT rate constant is lower than the PSI-VTST one. The calculated PSI-VTST rate constants for the $n = 1$–3 reactions overestimate the experimental values of Staneke *et al.*[9] by factors of 1.2 to 2.6. The computed rate constants for these reactions are all within a factor of 1.3 of each other, while the experimental values differ by as much as a factor of 1.8. The magnitude of overestimate for the $n = 1$ reaction could be due to classical recrossing, which is known to be important for these types of S_N2 reactions, and/or to inadequacies in the representation of the asymptotic potential by an electrostatic model. Note that an error of less than 1 kcal/mol in the free energy of activation leads to an error in the computed rate constant of over a factor of 3. The CVT rate constant for $n = 4$ underestimates the experimental rate constant by a factor of 170, which is equivalent to an error of 3 kcal/mol in the free energy of activation. Although this size of error in the barrier height cannot be totally discounted, it is larger than what we would expect from convergence of the reaction enthalpy and saddle point energy for the $n = 4$ reaction as shown in the benchmark calculations.

Rate constants for the microsolvated S_N2 reactions of $OH^- + CH_3Cl$ (Table 7) show that the dynamical bottlenecks for $m = 0$ is in the entrance channel, but shift to the saddle point region for $m > 0$. This finding is consistent with the fact that the saddle point energy (relative to the reactant energy) increases (becomes less negation) with increasing microsolvation. The minimum rate constants are in reasonable agreement with experiment for $m = 0$ and 1. For $m = 2$ only an upper bound to the rate constant was determined, and our computed rate constant is well below that value.

We have also initiated studies of the reactions of OH^- with chlorinated ethylenes. Figure 2 shows preliminary results for the reaction of OH^- with CH_2CHCl. Three reaction channels are possible. The first channel proceeds by proton transfer from the carbon atom with two hydrogen atoms and is monotonically downhill to the first complex, which is a water molecule hydrogen bonded to the $CHCHCl^-$ anion. There is a small barrier, relative to the energy of the complex, to dissociation of the chloride ion to form acetylene in a hydrogen bonded complex with water and Cl^-. The second channel proceeds by proton transfer from the carbon atom and is monotonically downhill to the complex of water with the CH_2CCl^- anion. This complex is lower in energy than the $CHCHCl^-(H_2O)$ complex, but the chloride elimination channel seen in the first channel is not energetically favorable in this case because of the formation of CH_2C:. The third channel is the S_N2 reaction, which is monotonically downhill in energy from the reactants to the $CH_2CHOH…Cl^-$ complex. Work is currently in progress on reaction with other $C_2H_{4-n}Cl_n$ molecules, future characterization of the reaction channels, and higher level calculations of the reaction energetics.

Hybrid HF-DF investigations

We began searching for accurate and affordable hybrid HF-DF methods first by studying reactions (R1) with $n = 1$ and 2. Table 8 compares the enthalpy of reaction at 0K, the energy of the reactant complex relative to the reactants, and the barrier height calculated at the MPW1K and MPW1KK levels of theory using various basis sets to these quantities calculated from experiment (for the enthalpy of reaction at 0K only) and high-level *ab intio* methods for reaction (R1) with $n = 1$. We make the same comparisons for reaction (R1) with $n = 2$ less the energy of the reactant complex relative to the energy of reactants in Table 9.
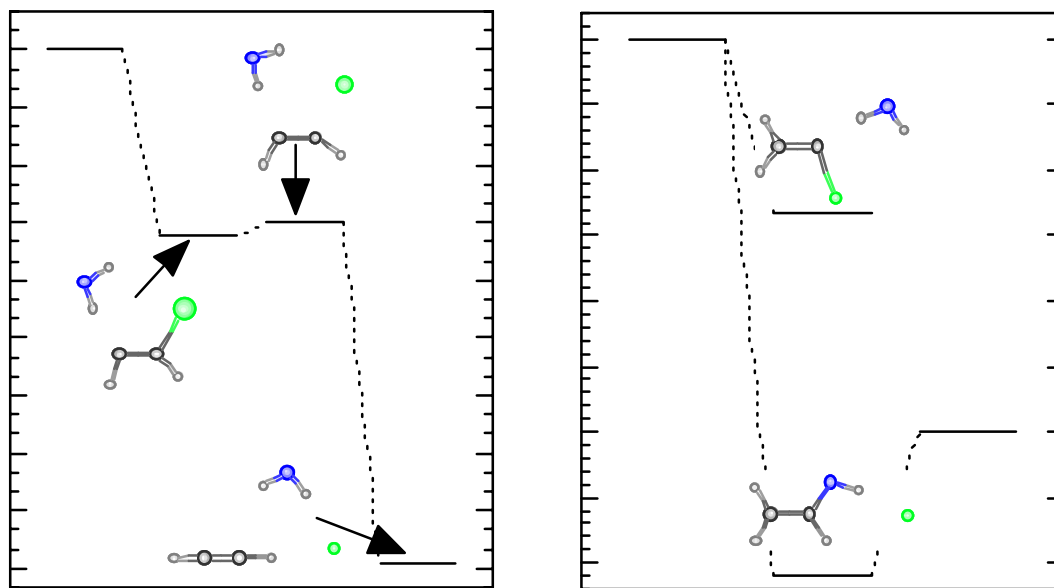
Figure 2. CCSD(T)/aVDZ//MP2/aVDZ energies at stationary points, relative to reactants, for the interaction of OH⁻ with CH₂CHCl. The left panel shows the energies for OH⁻ attack on the carbon atom with two hydrogen atoms and it displays a first complex, transition state and a final product complex. The right panel shows the energies for OH⁻ attack on the carbon atom with the chlorine atom and it displays a proton transfer complex (energy at 24 kcal/mol), S_N2 complex (lowest energy) and the final product energy for the S_N2 reaction.

Table 8. Energetics (Relative to the Reactants in kcal/mol) of Stationary Points for Reaction (R1) for $n = 1$.

level	Products[a]	reactant complex	saddle point
MPW1K/6-31+G(d)	-58.6	-17.5	-15.1
MPW1K/6-31+G(d,p)	-58.1	-17.9	-15.1
MPW1K/MG3	-55.6	-17.4	-14.2
MPW1KK/6-31+G(d)	-61.4	-17.6	-14.1
MPW1KK/6-31+G(d,p)	-60.8	-18.0	-14.0
MPW1KK/MG3	-58.2	-17.4	-12.9
MP2/MG3	-51.1		-13.5
MC-QCISD	-47.9	-15.0	-11.1
MC-G3	-49.4	-15.3	-12.8
Experiment[b]	-49.7 ± 1.2		

[a] Includes zero-point energy except for the MC-QCISD and MC-G3 levels of theory.
[b] Experimental reaction enthalpy at 0K.

Table 9. Energetics (Relative to the Reactants) of Stationary Points for Reaction (R1) with $n = 2$ (in kcal/mol)

level	Products[a]	saddle point
MPW1K/6-31+G(d)	-67.5	-16.6
MPW1K/6-31+G(d,p)	-66.9	-16.5
MPW1KK/6-31+G(d)	-70.3	-15.0
MPW1KK/6-31+G(d,p)	-69.8	-14.9
MP2/MG3	-58.0	-15.3
Experiment[b]	-58.7 ± 3.1	
(a) Includes zero-point energy.		
(b) Experimental reaction enthalpy at 0K.		

For reaction (R1) with $n = 1$, the MPW1K level of theory underestimates the enthalpy of reaction by 5.9-8.9 kcal/mol while MPW1KK underestimates the enthalpy of reaction by 8.5-11.7 kcal/mol. This would imply that a smaller fraction of HF exchange is required to accurately model these systems (if we consider the enthalpy of reaction as the only criterion with which to judge these electronic structure methods). The MPW1KK level of theory is approximately 1 kcal/mol closer to our best estimate of the barrier height (the MC-G3 level of theory) showing that there are opposing trends in the amounts of HF exchange required to get the barrier height and the enthalpy of reaction correct.

The same trends for the enthalpy of reaction at 0K and the barrier height that were observed for reaction (R1) are also observed for reaction (R1) with $n = 2$. Note that MP2/MG3 is currently our best estimate for the energetics of reaction (R1) with $n = 2$ and that this level of theory underestimates our best estimate of the barrier height by 0.7 kcal/mol for reaction (R1) with $n = 1$. It may be reasonable to assume that MP2/MG3 is underestimating the barrier height for reaction (R1) with $n = 1$ by approximately this amount as well. Thus for a given basis set, the barrier height at the MPW1KK level of theory is consistently better than the barrier height at the MPW1K level of theory by about 1.5 kcal/mol.

The fraction of HF exchange in the MPW1K level of theory was optimized to reproduce energies of reactions and barrier heights for a data set of 20 hydrogen atom abstraction reactions. This data set only contained neutral reactants, products, and saddle points. The reactions that we are studying in this research project contain negative ions, namely the hydroxide ion and the chloride ion. Although the MPW1K and MPW1KK levels of theory give good estimates of the barrier height for reaction (R1) with $n = 1$ and 2, they are not giving the same accuracy for the enthalpy of reaction (which is an important quantity to get right if we want to obtain accurate rate constants). We have therefore studied some simple reactions involving the hydroxide and chloride ions to determine if one or both of these ions are problematic for MPW1K and MPW1KK.

Table 10 compares the enthalpy of hydration at 298K of the hydroxide and chloride ion

$$OH^- + H_2O \rightarrow [OH(H_2O)]^- \qquad\qquad (R5)$$

$$Cl^- + H_2O \rightarrow [Cl(H_2O)]^- \qquad\qquad (R6)$$

calculated at the MPW1K and MPW1KK levels of theory to experiment (for reaction (R5) only) and to MP2/MG3. Table 10 also presents a comparison of electron affinities calculated from the MPW1K and MPW1KK levels of theory to experiment and to MP2/MG3. The MP2/MG3 level of theory underestimates the experimental enthalpy of hydration at 298K of the hydroxide ion by 2.7 kcal/mol. For a given basis set, the MPW1K and MPW1KK levels of theory underestimate the enthalpy of hydration of the hydroxide ion by an additional 1.1-2.3 kcal/mol and 0.8-1.7 kcal/mol, respectively. On the other hand, the MPW1K and MPW1KK levels of theory agree within 0.1 kcal/mol of the MP2/MG3 prediction of the enthalpy of hydration of the chloride ion. From the comparison of electron affinities we observe that the major source of error with MPW1K and MPW1KK for reactions (R1) may be associated with the hydroxide ion.

Table 10. Enthalpies of Hydration, ΔH_{298}, and Electron Affinities for the Hydroxide and Chloride Ions (in kcal/mol).

level	ΔH_{298}		Electron Affinities	
	OH^-	Cl^-	OH^-	Cl^-
MPW1K/6-31+G(d)	-30.3	-14.6	30.3	81.5
MPW1K/6-31+G(d,p)	-31.5	-14.6	31.0	81.5
MPW1K/MG3			31.0	80.1
MPW1KK/6-31+G(d)	-30.0	-14.6	26.0	80.7
MPW1KK/6-31+G(d,p)	-30.9	-14.5	26.7	80.7
MPW1KK/MG3			26.6	79.1
MP2/MG3	-29.2	-14.7	42.7	81.8
Experiment	-26.5 ± 1.0		42.2	83.4

ONIOM Study of Chemical Reactions in Micro-solvation Clusters

The reliability of the two-layered ONIOM (our own N-layered molecular orbital + molecular mechanics) method was examined for the investigation of the S_N2 reaction pathway (reactants, reactant complexes, transition states, product complexes and products) between CH_3Cl and OH^- ion in micro-solvation clusters with one or two water molecules.

$$OH^-(H_2O)_m + CH_eCl(H_2O)_k \rightarrow CH_3OH(H_2O)_{m'} + Cl^-(H_2O)_{k'} \qquad\qquad (R7)$$
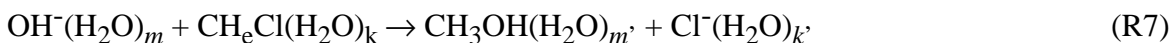
Only the solute part, CH_3Cl and OH^-, was treated at a high level of molecular orbital (MO) theory and all solvent water molecules at a low MO level.

The ONIOM calculation at the MP2(Møller-Plesset second order perturbation)/aug-cc-pVDZ (augmented correlation-consistent polarized valence double zeta basis set) level of theory as the high level coupled with the B3LYP (Becke3 parameter-Lee-Yang-Parr) /6-31+G(d) as the low level was found to reasonably reproduce the "target" geometries at the MP2/aug-cc-pVDZ level of theory. As shown in Tables 12, the energetics can be further improved to an average absolute error of < 1.0 kcal/mol per solvent water molecule relative to the "target" CCSD(T) (coupled cluster singles and doubles with triples by perturbation) /aug-cc-pVDZ level by using the ONIOM method in which the high level was CCSD(T)/aug-cc-pVDZ level with the low level of MP2/aug-cc-pVDZ. Further details of these calculations are presented elsewhere.[5]

We have documented timing data for $(CH_3Cl)(H_2O)$ and $(CH_3Cl)(H_2O)_2$ using a PC with an Intel Pentium II CPU, as shown in Table 14. For the m+n=1 system, the cost of ONIOM geometry optimization is about 20% of the pure MO optimization, and the cost of single point improved energy calculation is about 10% of the pure MO calculation. For m+n=2 system, this ratio decreases to 10% and less than 2%, respectively. If B3LYP is used in the single point calculation instead of MP2, the decrease in the cost ratio will be even more dramatic. These ratios will decrease further with $m + k > 2$.

The present results indicate that the ONIOM method would be a powerful tool for obtaining reliable geometries and energetics for chemical reactions in larger micro-solvated clusters with a fraction of cost of the full high level calculation, when an appropriate combination of high and low level methods is used. The importance of careful tests is emphasized.

---

[5] S. Re and K. Morokuma, J. Phys. Chem. A **105**, 7185 (2001).

Table 12. Calculated Relative Energies (in kcal/mol) of Reaction (R7) with $m + k = 1$ and 2 Obtained at CCSD(T)/aug-cc-pVDZ//MP2/aug-cc-pVDZ (CC/b//MP2/b) Level of Theory and Various ONIOM Levels at the IMOMO(MP2/b:B3LYP) Optimized Geometries.[a]

	Pure MO	ONIOM					
	CC/b//	MO		IMOMO		IMOMO	
	MP2/b[b]	CC/b		(CC/b:MP2)		(CC/b:B3LYP)	
		$m + k = 1$					
$OH^- + CH_3Cl \cdot (H_2O)$	22.6	22.6	(0.0)	23.6	(1.0)	26.4	(3.8)
$OH^- \cdot (H_2O) + CH_3Cl$	0.0	0.0		0.0		0.0	
$[CH_3Cl\cdots OH^-] \cdot H_2O$ (**RC1**)	-14.7	-14.7	(0.0)	-14.3	(0.4)	-13.2	(1.5)
$[Cl^-\cdots CH_3\cdots OH]^- \cdot H_2O$ (**TS1**)	-9.1	-8.9	(0.2)	-9.8	(-0.7)	-7.4	(1.7)
$[Cl^-\cdots CH_3OH] \cdot H_2O$ (**PC1**)	-58.4	-58.2	(0.2)	-58.6	(-0.2)	-55.2	(3.2)
$H_2O + CH_2Cl^- \cdot (H_2O)$	13.6	14.0	(0.4)	12.2	(1.4)	13.5	(-0.1)
$Cl^- + CH_3OH \cdot (H_2O)$	-32.9	-32.9	(0.0)	-33.3	(-0.4)	-30.7	(2.2)
$Cl^- \cdot (H_2O) + CH_3OH$	-41.4	-41.4	(0.0)	-41.2	(0.2)	-39.0	(2.4)
averaged absolute error			(0.1)		(0.6)		(2.2)
		$m + k = 2$					
$OH^- + CH_3Cl \cdot (H_2O)_2$	40.7	40.8	(0.1)	44.4	(3.7)	47.9	(7.2)
$OH^- \cdot (H_2O) + CH_3Cl \cdot (H_2O)$	17.8	17.9	(0.1)	20.4	(2.6)	21.0	(3.2)
$OH^- \cdot (H_2O)_2 + CH_3Cl$	0.0	0.0		0.0		0.0	
$[CH_3Cl\cdots OH^-] \cdot 2H_2O$ (**RC2**)	-13.1	-13.5	(-0.4)	-12.1	(1.0)	-10.7	(2.4)
$[Cl^-\cdots CH_3\cdots OH]^- \cdot 2H_2O$ (**TS2c**)	-2.1	0.1	(2.2)	-0.4	(1.7)	1.9	(4.0)
$[Cl^-\cdots CH_3\cdots OH]^- \cdot 2H_2O$ (**TS2s**)	-4.0	-3.8	(0.2)	-4.4	(-0.4)	-1.1	(2.9)
$[Cl^-\cdots CH_3OH] \cdot 2H_2O$ (**PC2**)	-49.9	-49.6	(0.3)	-48.6	(1.3)	-44.2	(5.7)
$Cl^- + CH_3OH \cdot (H_2O)_2$	-21.8	-21.6	(0.2)	-21.9	(-0.1)	-18.9	(2.9)
$H_2O + CH_2Cl^- \cdot (H_2O)_2$	26.9	24.8	(-2.1)	25.8	(-1.1)	29.7	(2.8)
$Cl^- \cdot (H_2O) + CH_3OH \cdot (H_2O)$	-25.4	-25.3	(0.1)	-24.1	(1.3)	-21.4	(4.0)
$Cl^- \cdot (H_2O)_2 + CH_3OH$	-34.5	-34.3	(0.2)	-32.7	(1.8)	-29.9	(4.6)
averaged absolute error			(0.6)		(1.5)		(4.0)

(a) The numbers in parentheses are the differences from the target CC/b//MP2/b calculation.

(b) The target calculation

(c) CC = CCSD(T)/aug-cc-pVDZ; MP2/b = MP2/aug-cc-pVDZ; MP2 = MP2/6-31+G(d); B3LYP = B3LYP/6-31+G(d).

Table 14. Timing Data (in s) for ONIOM (MP2/b:B3LYP) Calculations Compared with Pure MP2/b calculations.[a]

	MP2/b	ONIOM
Geometry optimization (per cycle)		
$(CH_3Cl)(H_2O)$	5544	1178
$(CH_3Cl)(H_2O)_2$	15782	1602
Single point calculation		
$(CH_3Cl)(H_2O)$	16440	1629
$(CH_3Cl)(H_2O)_2$	104965	1922

(a) Calculated using an Intel Pentium II CPU.